Article

Not peer-reviewed version

P311 Curtails Inflammation Through M2-Type Polarization of Macrophages and Potentially via Gut Microbiome Modulation

Steven Moreton , Sreenu Boddupally , Pavana Jyothsna Kasaram , Kameswara Rao Badri *

Posted Date: 22 April 2026

doi: 10.20944/preprints202604.1556.v1

Keywords: P311; inflammation phenotypes; dysbiosis; M2-type macrophage polarization; obesity

 doi:10.20944/preprints202604.1556.v1

Article

P311 Curtails Inflammation Through M2-Type Polarization of Macrophages and Potentially via Gut Microbiome Modulation

Steven Moreton [1,2,†], Sreenu Boddupally [2,3,†], Pavana Jyotsna Kasaram [2,†] and Kameswara Rao Badri [1,2,*]

[1] Department of Pharmacology & Toxicology

[2] Cardiovascular Research Institute, Morehouse School of Medicine, Atlanta, GA 30310, USA

[3] Current address: Tulsi Therapeutics, NIMS, Hyderabad, Telangana, India

* Correspondence: kbadri@msm.edu; Tel.: +1-404-756-5025

† Equal contributing authors.

Abstract

Adipose tissue is a heterogenous organ with newly identified endocrine function, consisting of immune cells along with main populations of fat storing adipocytes and adipose precursor cells. Dysregulated immune cell function and infiltration cause low grade chronic inflammation in adipose tissue that leads to various metabolic disorders like obesity, insulin resistance, type2 diabetes and cardiovascular disease. Our research showed the role of P311 protein in adipogenesis, amoeboid migration, vascular wall homeostasis, and blood pressure regulation. Studies from our laboratory and other labs showed the potential involvement of P311 in wound healing and predicted immune function. Here we studied the role of P311 on inflammation mainly focusing on macrophage phenotypes and functions as macrophages are predominant immune cells in adipose tissue that switch the inflammatory micro-environment between pro- and anti-inflammatory conditions. For the first time, we show the expression of P311 in macrophages implicating its role in inflammation directly. Further, P311 expression in macrophages induced anti-inflammatory phenotype (M2 macrophages) through phosphorylation of STAT6 of canonical JAK/STAT signaling pathway. The human gastrointestinal (GI) system harbors high populations of both healthier and pathogenic microbial communities that provide immunity, inflammation, nutrients, and GI tract epithelial homeostasis. Given the roles of P311 in macrophage mediated inflammation and metabolic diseases, we verified whether lack of P311 in P311 knockout mice has any effects on GI microbiome compared to wildtype mice. Our studies demonstrate that lack of P311 led to changes in the intestinal microbial strains. Together, current studies implicate a larger role of P311 connecting inflammation and microbiome with obesity.

Keywords: P311; inflammation phenotypes; dysbiosis; M2-type macrophage polarization; obesity

1. Introduction

Obesity is a chronic low grade inflammatory disease, mainly thought to be caused by imbalance in energy homeostasis of body caused by excessive dietary intake and reduced energy expenditure. This leads to excess accumulation of body fat. However, lately multiple genetic, environmental, and biological factors involved in obesity have been identified indicating the importance of addressing this pandemic[1]. Obesity will have a negative impact on individuals' health with serious morbidity and mortality, leaving a financial burden on the individuals, family, as well as affecting health metrics at the national level. Individuals' weight status including overweight and obesity is classified based on the Basal Metabolic Index (BMI) of the individuals, which will be calculated using a person's weight and height. Based on the individuals BMI(kilogram/m^2, The National Institute of Health

 doi:10.20944/preprints202604.1556.v1

(NIH) classification), a person can be underweight (BMI <18.5), normal weight (BMI 18.5 – 24.9), overweight (BMI 25 – 29.9), Class 1 obese (Low-risk; BMI 30-34.9), Class 2 obese (Moderate-risk; BMI 35-39.9) and Class 3 obese (Severe/morbid; BMI >40). However, measurements such as BMI is not entirely sufficient for classifying a person as obese or malnourished [2,3]. Increased BMI correlates with individuals found to be overweight and are at increased overall risk for obesity-related comorbidities and increased morbidity and mortality [4]. Obesity is a risk factor for various metabolic and metabolic-associated diseases such as insulin resistance, type 2 diabetes mellitus (T2DM), cardiovascular disease, hypertension, stroke, and liver disease [4–6]. The prevalence of obesity in United States has been increasing dramatically in last two decades, it has increased from 30.5% to 41.9% among US adults aged 20 or over and severe obesity increased from 4.7% to 9.2%as per 2017-2020 report[7].

Physiologically, obesity disrupts metabolic functions of the body, primarily with increased quantity and decreased quality of adipose tissue leading to imbalance in glucose regulation and lipid metabolism. This further leads to the release of excess free fatty acids and proinflammatory cytokines into circulation. Adipose tissue is majorly composed of adipocytes or fat cells that store excess energy in the form of lipids. In addition, adipose tissue contains heterogenous cell populations including precursor cells, endothelial cells, fibroblasts, and immune cells such as neutrophils, eosinophils, dendritic cells, mast cells innate lymphoid cells, macrophages, natural killer cells and activated T and B lymphocytes [8–10]. In lean conditions, diverse immune cells function harmoniously and maintain adipose tissue homeostasis. In overweight and obesity conditions, excess lipid accumulation and metabolic stress disrupts this homeostasis, leading to inflammation and adipose tissue disfunction [11,12]. Among different immune cells in adipose tissue, macrophages are most abundant cell population constituting 5-10% cells of the adipose tissue in lean condition. However, these numbers of macrophages increase significantly to 50% or more in obese and extreme obesity conditions accelerating inflammation [13].

Macrophages displays wide range of cell surface markers that recognizes damage associated molecular patterns (DAMPs) and pathogen associated molecular patterns (PAMPs) by different pattern recognition receptors (PRRs) such as Toll like receptors (TLRs) and Nod like receptors (NLRs). Binding to receptors trigger intra cellular signaling that alters gene expression and production of cytokines [14]. There are several phenotypes of macrophages in humans and mice that can be identified based on their cell surface markers and biological activity. Two major phenotypes of macrophages are classically activated or inflammatory (M1) macrophages and alternatively activated or anti-inflammatory (M2) macrophages [15–17]. Additional types of macrophages, lipid associated macrophages, and metabolic associated macrophages participate in other mechanisms of metabolism. Pathogen associated lipopolysaccharides (LPS) as well as a cytokine of Th1 i.e., interferon γ (IFN-γ) are known to activate the naïve macrophages to M1 phenotype. These macrophages show enhanced phagocytic activity, acts against infection and inflammation by increased secretion of proinflammatory cytokines such as TNF-α, IL-1β, IL-6, IL-12, chemokines CXCL10, CXCL11 and low levels of IL-10 [18]. Macrophages that are alternatively activated with Th2 cytokines such as IL-4 and/or IL-13 polarize native macrophages to M2 phenotypes. These macrophages are charactered by increased mitochondrial respiration and secretion of anti-inflammatory cytokines such as IL-10 and TGF-β, involved in scavenging debris, cell apoptosis, tissue repair, and wound healing [19,20].

Apart from M1 and M2 phenotypes, adipose tissue macrophages (ATMs) exist with additional features based on several factors in the adipose tissue microenvironment. Macrophages form crown-like structures (CLS) and uniquely express chemokine receptors to clear lipid filled /dead adipocyte in adipose tissue [21]. In dysregulated adipose microenvironment, hypertrophied adipocytes release multiple proinflammatory cytokines, mainly monocyte chemoattractant protein I (MCP1), which initiates the infiltration of macrophages. Traumatized adipose tissue environment filled with abundant glucose, very low-density lipoproteins, and short chain fatty acids alter macrophage phenotype and enhance the secretion of proinflammatory cytokines.

 doi:10.20944/preprints202604.1556.v1

Macrophages show high plasticity, which can polarize switching to different phenotypes in response to various micro-environmental stimuli and signals from pathogens [22,23]. However, there is growing evidence show that microbiome of organs and organ systems are associated with immunity and inflammation. The microbiome is an essential aspect of human physiology, performing multiple functions related to metabolism, immunity, and inflammation along with other functions like nutrient absorption and vitamin production. The microbes associated with human organs and organ systems including gastrointestinal (GI) tract are taxonomically diverse, consisting of various bacteria, archaea, fungi, protozoa, and viruses [24,25]. More specifically, the microbes of the gut reported to have a key role in metabolisms through breakdown of complex carbohydrates, starches, fats, and sugars, some of which are indigestive without the assistance of these microbial communities. The gut microbiome aids in absorbing energy from these compounds to power the bodily processes. Relatedly, gut microbial communities produce essential vitamins such as Vitamin B and K that cannot be produced endogenously without these microbes, which makes the microbiome presence indispensable [26]. Though functionally diverse, these communities work synergistically to help to maintain the body's overall energy homeostasis as well as immunity and inflammation[27]. In line with this, microbes modify the gut environment by maintaining the integrity of the gastrointestinal lining and GI functioning through the release of bio-metabolites which modify the capacity of the digestive enzymes and fluids to break down structurally complex compounds [28]. Furthermore, microbes provide defense against pathogens or opportunistic bacteria by releasing peptides and metabolites which inhibit their growth and presence in the gut and their leakage into the body to affect at system level [26].

One of the challenges in the study of gut microbiome and microbial dynamics is the characterization of the diversity in microbial communities in these spaces. There are many factors to consider when attempting to describe the complexity of the microbial ecosystem, such as incomplete annotation schemes for poorly described species or proper labeling of organisms which are phylogenetically similar. Compounding these factors are genetic changes that occur such as gene duplication, gene transfer, and gene fusion that alter the genetic code making identification of these species even more challenging [29]. Gene sequencing has greatly assisted in this task making large scale analysis of microbial ecosystems feasible. Whole Genome Sequencing (WGS) or the shotgun method sequences the entire DNA of a sample, providing a broad overview of the microbial community with high-resolution strain-level identification but at a higher cost and data complexity [30]. Whereas 16S rRNA sequencing amplifies the variable region V3-V4, a sequence approximately 540 base pairs long, located in a region that is genetically heterogenous and provides a distinguishable and is statistically capability to separate organisms up to the genus/species level. This method is financially more cost effective and requires less computational power [31].

P311 protein is a small protein with 68 amino acids (8kDa) also known as neuronal regeneration-related protein (NREP), C5orf13, D4S114, PRO1873, PTZ17, SEZ17. Our protein modeling studies along with circular dichroism studies showed that P311 is a novel intrinsically disordered protein [32]. It is conserved across the species and present in various cells and cellular processes like vascular smooth muscle homeostasis, fibroblast activation to myofibroblasts, neural regeneration, blood mononuclear cells, adipocytes and lung tissues (injury and repair) [33–41]. Other studies showed the significant role of P311 protein cell development, migration, and differentiation. P311 promotes ameboid-like cell migration of activated fibroblasts or myofibroblasts through RalA activation [38]. Our and other studies reported that P311 has a role in adipogenesis [32,36] through transcriptional regulation of PPAR γ [32]. *In silico* studies implicated potential role of P311 in inflammation through protein-protein interaction network model and was established in wound healing studies [34,38,42]. However, systematic studies are needed to understand the role of P311 and its molecular mechanisms in different disease conditions especially P311/macrophages/dysbiosis/obesity axis. Considering adipose tissue and macrophage cross talk in metabolic conditions, we initiated the current study to understand the role of P311 on macrophage homeostasis. In addition, we studied the effect of lack of

 doi:10.20944/preprints202604.1556.v1

P311 on the gut microbiome of the mouse to understand possible relation between gut microbiome and obesity/inflammation.

2. Results

2.1. Expression of P311 and Macrophage Markers in Dose Dependent and Time Dependent Treatment of RAW 264.7 Cells with LPS and IL4

Macrophages exhibit high plasticity, based on environment and stimulants, and they differentiate either into pro-inflammatory phenotype (M1 macrophages) or anti-inflammatory phenotypes (M2 macrophages). Here, we used LPS as a potent proinflammatory macrophage inducer [43,44] and IL4 is a potent inducer of macrophages to M2 phenotype with anti-inflammatory roles [45]. We conducted these dose and time dependent experiments to verify the expression of P311 in RAW cells that also led us to optimize concentration and time of treatment of LPS or IL4. Different concentration of LPS; 0, 10, 25, 50, 100 and 200 ng/mL were used, and the cells were treated for 24 hours. Later, verified the expression of P311, CD86 (M1 macrophage marker, pro-inflammatory phenotype) and CD68 (pan macrophage marker and CLS marker) by qPCR and western blot analysis. Figure 1 shows that the dose dependent treatment of LPS increased CD86 expression both at the level of mRNA and protein expression as expected. But CD68 data showed no difference at transcripts level, however a small decrease in CD68 expression was shown with the treatment of LPS. Endogenous P311 expression was reduced as observed in qPCR studies in LPS treated group compared with control group (vehicle treated 0 ng/mL group). Based on our current data and other publications [46], we chose LPS at a concentration of 100 ng/mL as optimal concentration for future studies.

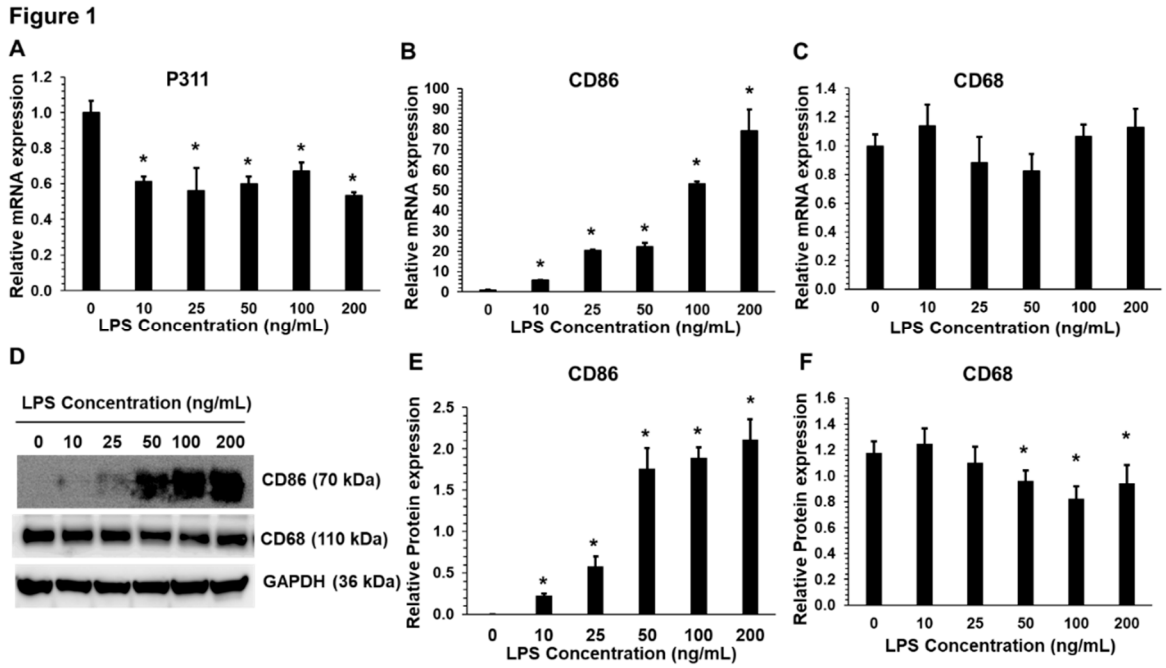

Figure 1. Dose dependent lipopolysaccharide (LPS) treatments induced M1-type macrophage polarization but decreased expression of P311 in RAW 264.7 cells. A-C. qPCR was used to study the dose dependent effect of LPS on the expression of P311 (A), CD86 (B) and CD68 (C). D. Immunoblot analyses was performed to verify the expression of CD86 (M1 marker) and CD68 (Pan-macrophage marker). Lower panel represents loading control, GAPDH. E-F. Densitometric quantitation of CD86 and CD68 proteins expression normalized to GAPDH expression. qPCR data reported as ΔΔ CT method normalized with TATA-binding protein (TBP). Histograms represents mean ± S.D. *Represents statistical significance ($p<0.05$) between 0 ng/mL vs. different concentrations of LPS treatments.

 doi:10.20944/preprints202604.1556.v1

Figure 2 shows the expression of P311, CD86 and CD68 with the treatment of LPS (100 ng/mL) for different time exposures; 0, 4, 9, 24, 48 and 72 hours. The data showed maximum expression of CD86 at 24-48 hours after treatment. However, CD68 expression was significantly decreased at 48 and 72 hours. However, the P311 expression was increased with time after treating with LPS. From these studies, we chose LPS treatment at a concentration of 100 ng/mL for 24 hours as optimal dose and time to study M1-macrophage characterization.

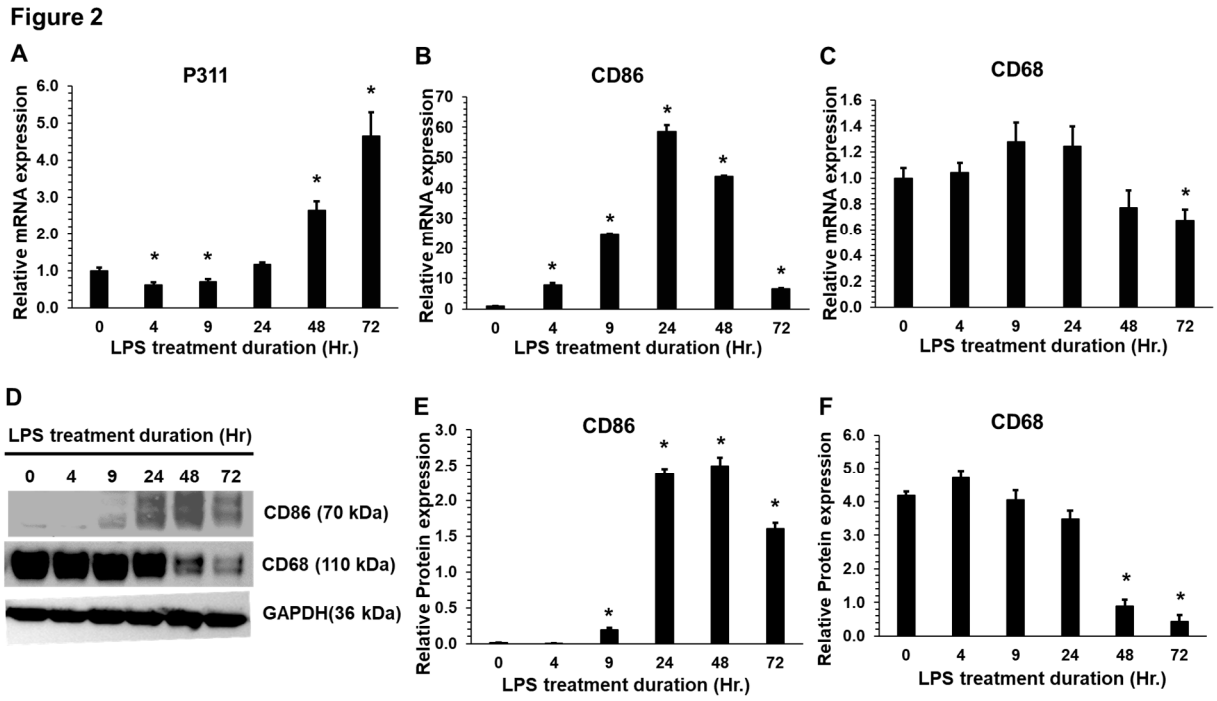

Figure 2. Time dependent lipopolysaccharide (LPS) treatments induced M1-type macrophage polarization and expression of P311 in RAW 264.7 cells. A-C. qPCR was used to study the time dependent effect of LPS on the expression of P311 (A), CD86 (B) and CD68 (C). D. Immunoblot analyses was performed to verify the expression of CD86 (M1 marker) protein and CD68 (Pan-macrophage marker) protein. Lower panel represents loading control, GAPDH. E-F. Densitometric quantitation of CD86 and CD68 proteins expression normalized to GAPDH expression. Histograms represents mean ± S.D. *Represents statistical significance ($p<0.05$) between 0 hour (hr) vs. different hours of LPS treatment.

Further, we studied the effect of anti-inflammatory macrophage phenotype inducer, Il4 treatment at different concentrations i.e., 0, 2, 5, 10, 20 and 50 ng/mL for 24 hours on RAW cells (Figure 3). After the treatment, the cells were harvested and verified the expression of CD206 (M2-macrophage phenotype marker, anti-inflammatory) and CD68 along with P311 using qPCR and western blot analysis. Figure 3 shows our results with increased expression of CD206 at mRNA level and protein level at all concentrations of IL4 assessed, from 2 ng/mL to 50ng/mL. However, CD68 protein expression was increased with the increase in the concentration of IL4 treatment without any change in transcript expression. The P311 transcript levels increased significantly with the treatment of IL4 at all concentrations compared to control group with maximum expression at 10ng/mL concentration. Furthermore, time dependent treatment studies at 0, 4, 9, 24, 48 and 72 hours with IL4 at a concentration of 10 ng/mL showed significant increase in the expression of CD206 at 24 to 72 hours after treatment both at protein and transcript levels. There is no change in the CD68 levels. P311 transcript levels significantly increased from 4 hours to 72 hours compared to control group. From these studies, we chose IL4 treatment at a concentration of 10 ng/mL for 48 hours as optimal dose and time to study M2 macrophage phenotype characterization.

 doi:10.20944/preprints202604.1556.v1

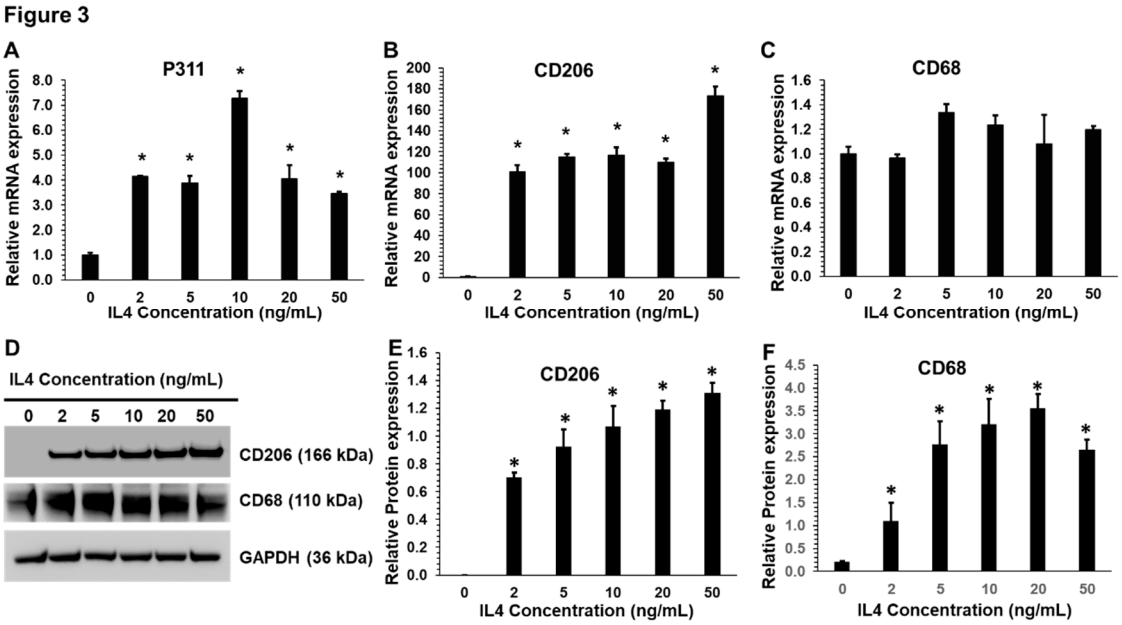

Figure 3. Dose dependent interleukin (IL)-4 treatments induced M2-type macrophage polarization and expression of P311 in RAW 264.7 cells. A-C. qPCR was used to study the dose dependent effect of IL4 on the expression of P311 (A), CD206 (B) and CD68 (C). D. Immunoblot analyses was performed to verify the expression of CD206 (M2 marker) and CD68. Lower panel represents loading control, GAPDH. E-F. Densitometric quantitation of CD206 and CD68 proteins expression normalized to GAPDH expression. qPCR data reported as ΔΔ CT method normalized with TATA-binding protein (TBP). Histograms represents mean ± S.D. *Represents statistical significance ($p<0.05$) between 0 ng/mL vs. different concentrations of IL4 treatments.

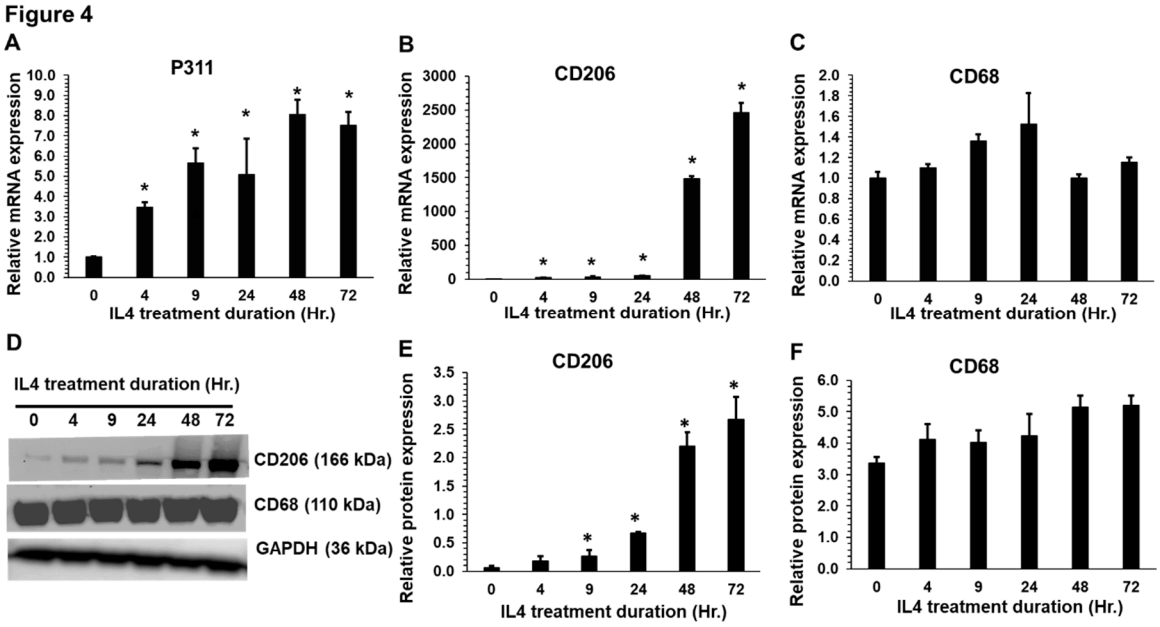

Figure 4. Time dependent interleukin (IL)-4 treatments induced M2-type macrophage polarization and expression of P311 in RAW 264.7 cells. A-C. qPCR was used to study the time dependent effect of IL4 on the expression of P311 (A), CD206 (B) and CD68 (C). D. Immunoblot analyses was performed to verify the expression of CD206 (M2 marker) protein and CD68 protein. Lower panel represents loading control, GAPDH. E-F. Densitometric quantitation of CD206 and CD68 proteins expression normalized to GAPDH expression. Histograms represents mean ± S.D. *Represents statistical significance ($p<0.05$) between 0 hour vs. different hours of IL4 treatment.

 doi:10.20944/preprints202604.1556.v1

2.2. P311 Is Expressed in Macrophages

As we did not see the expression of P311 in regular immunoblot studies (with 30ug lysates input) potentially due low abundance and short half-life of P311 despite use of proteasomal degradation inhibitor and protease inhibitors, we verified the expression of endogenous P311 using flow cytometry and immunofluorescence. Figure 5 shows the flowcytometry and immune blots analyses (protein input, 80-100µg) of RAW cells treated with different concentrations of LPS (100 ng/mL and 250 ng/mL) and IL4 (10 ng/mL and 25ng/mL) along with vehicle treatment as control for 24 hrs. Figure 5A-B shows the flowcytometry data with a noticeable decrease in P311 expression with LPS treatments (Q2- $F4/80^{+}P311^{+}$, 11.2% and 7.3% cells) whereas as IL4 treated RAW cells group showed a concentration dependent increase in P311 expression (Q2 - 19.6% and 25.1% of $F4/80^{+}P311^{+}$ cells) in treated macrophages ($F4/80^{+}$). Figure 5C show the expression of P311 protein bands in only IL4 treated group of raw cells, but not in LPS treated and control groups. Lysates of pcP311 transfected cell lysates are used as positive control. Expression of TATA-binding protein (TBP) was used as loading control.

Figure 5

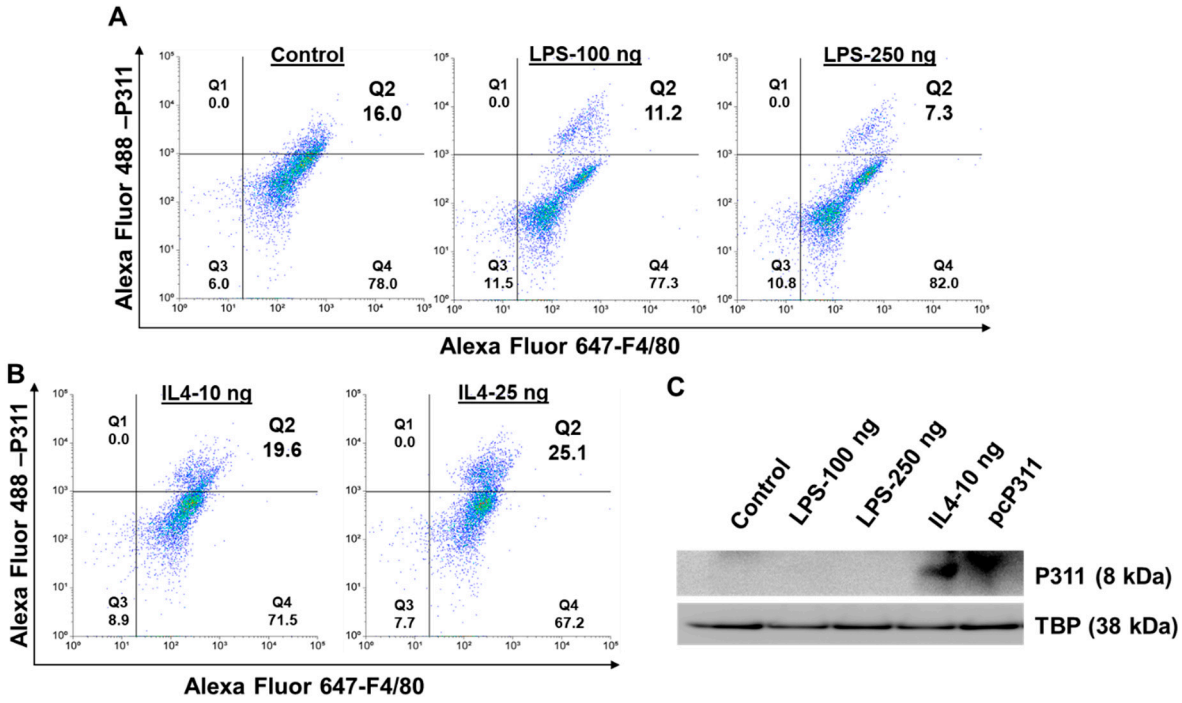

Figure 5. P311 protein is expressed in Raw 264.7 cells. A-B. Flowcytometric analyses of expression of P311 in Raw macrophages with no treatment control (A, left panel), 100 ng of LPS (A, middle panel), 250 ng (A, right panel) of LPS, 10 ng of IL4 (B, left panel) and 25ng of IL4 (B, right panel). B: Immunoblot analyses was performed to verify the expression of P311 in RAW cells treated with LPS and IL4. Lower panel represents loading control, TBP.

Complementing flow cytometry and immunoblot studies, we conducted immunofluorescence (IF) studies for P311 expression. Figure 6 show the IF images of the endogenous P311 expression in RAW cells treated with vehicle (control), LPS and IL4. IL4 treatment showed increased P311 (green color florescence), whereas LPS showed decrease in P311 expression. However, some basal expression of P311 was observed in control untreated group of RAW cells in FACS studies. Figure 6B shows the quantification of immunofluorescence of P311 (green) normalized to cell numbers (blue fluorescence). Collectively these experiments showed the expression of endogenous P311 protein in macrophages for the first time. In addition, these studies implicate the potential role of P311 in macrophage phenotype switching depending on the microenvironment (type, concentration, and time of treatments of stimulants).

 doi:10.20944/preprints202604.1556.v1

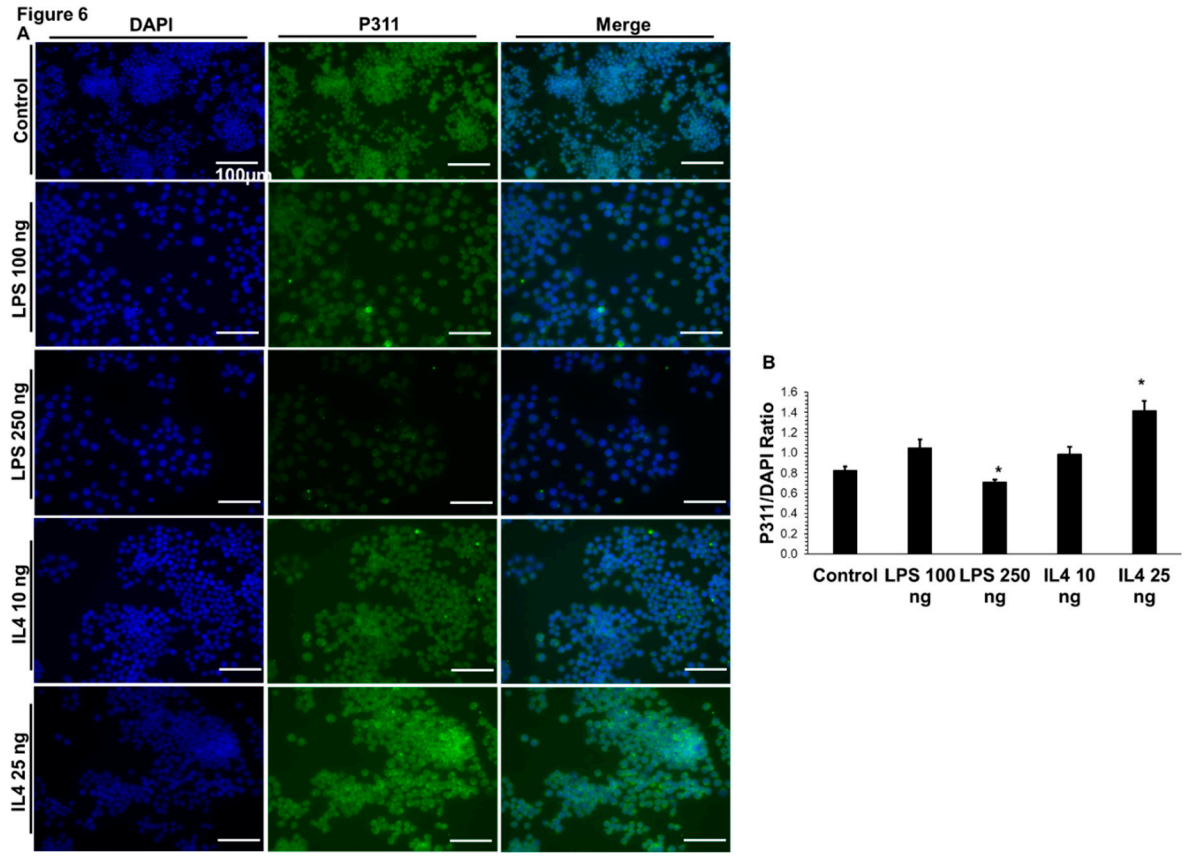

Figure 6. P311 protein is expressed in Raw 264.7 cells. A: Immunofluorescence analysis of P311 (Green) and nuclear stain, DAPI (Blue) in untreated control cells (A, top panel), LPS (A, 2nd, and 3rd panels) and IL4 (A, 4th, and 5th panels) treated Raw cells. B: Densitometric quantitation of P311 expression (green fluorescence) normalized to cell numbers (blue fluorescence). Histograms represents mean ± S.D. *Represents statistical significance ($p<0.05$) between control vs. different concentrations of treatments. All the IF pictures represent 40X magnification.

2.3. Overexpression of P311 Induce M2-Type Macrophage Cell Activation

To study the effect of P311 on macrophage polarization, we verified the expression of M2-macrophage marker, CD206 and M1-macrophage marker CD86 in empty vector and c-myc-tag P311 overexpressing pcP311 transfected RAW cells using lipofectamine 3000. We verified for the macrophage phenotype switch using surface markers CD68, CD86 and CD206 by qPCR, western blotting, and FACS analysis (Figure 7). Figure 7 show the expression of CD206, CD86 and CD68 transcripts using qPCR and P311, CD206, CD86 and CD68 protein expression using immunoblots in RAW cells transfected with pCMV and pcP311. c-myc-tag P311 overexpressing cells showed a significant increase in M2-macrophage marker (CD206) and decrease in M1-macrophage marker (CD86). However, there is no difference in the expression of CD68 marker. α-tubulin was used as loading control and P311 overexpression was verified with c-myc tag anti-body. Figures E, F and G show the quantification of western blot bands shown in figure D for CD206, CD86 and CD68, respectively. These studies were complemented with flow cytometry analyses (Figure 6H-J) that showed increase in P311+ cells (14.6%), decrease in $CD86^+$ cells (10.3%; Q2- myc^+CD86^+) and increase in CD206+ cell population (12.6%; Q2-myc^+CD206^+) in pcP311 transfected group respectively when compared to control empty vector (pCMV) transfected group.

 doi:10.20944/preprints202604.1556.v1

Figure 7

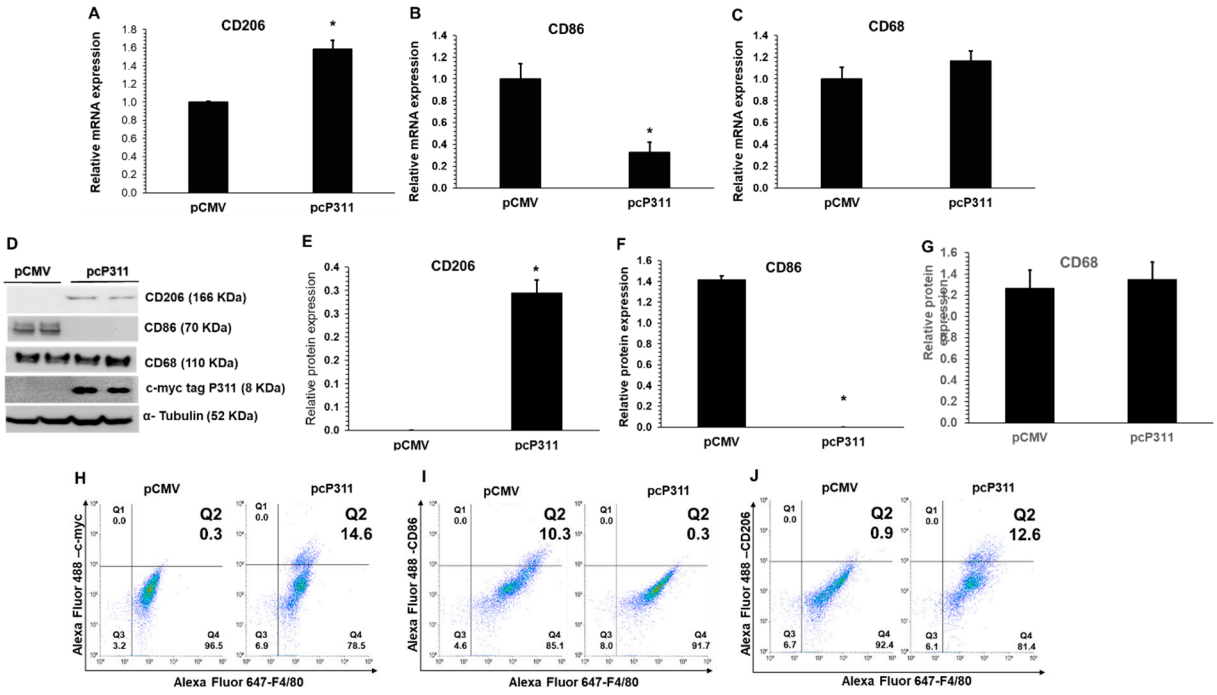

Figure 7. Overexpression of P311 induced M2-type macrophage polarization and reduced M1-type macrophage polarization. A-C. qPCR was used to study the overexpression of c-myc-tag-P311 on the expression of CD206 (A), CD86 (B), and CD68 (C) compared to empty vector control (pCMV) transfected RAW cells. D. Immunoblot analyses was performed to verify the expression of CD206 (M2 marker), CD86 (M1 marker) and CD68 (pan macrophage marker). C-myc-tag-P311 expression was detected using c-myc tag antibody. Lower panel represents loading control, α-tubulin. E-G. Densitometric quantitation of CD206, CD86 and CD68 proteins expression normalized to α-tubulin expression. H-J: Flowcytometric analyses of macrophage markers (CD206 and CD86) expression with c-myc-tag-P311 expression in pcP311 transfected and empty vector (pCMV) transfected control RAW cells. Expression c-myc-tagged P311 (H), CD86 (I) and CD206 (J) were shown in F4/80 gated RAW cells transfected with pCMV and pcP311. qPCR data reported as $\Delta\Delta$CT method normalized with TATA-binding protein (TBP). Histograms represents mean ± S.D. *Represents statistical significance ($p<0.05$) between pcP311 vs. pCMV group.

Figures 8 show the evaluation of P311 overexpression in RAW cells treated with IL4 and LPS. After 16 hours of (overnight) transfection, with pCMV and pcP311, Raw cells were incubated with 10 ng/mL of IL4 or 100 ng/mL of LPS for 24 hours. Cells were harvested for immune blot analysis.

 doi:10.20944/preprints202604.1556.v1

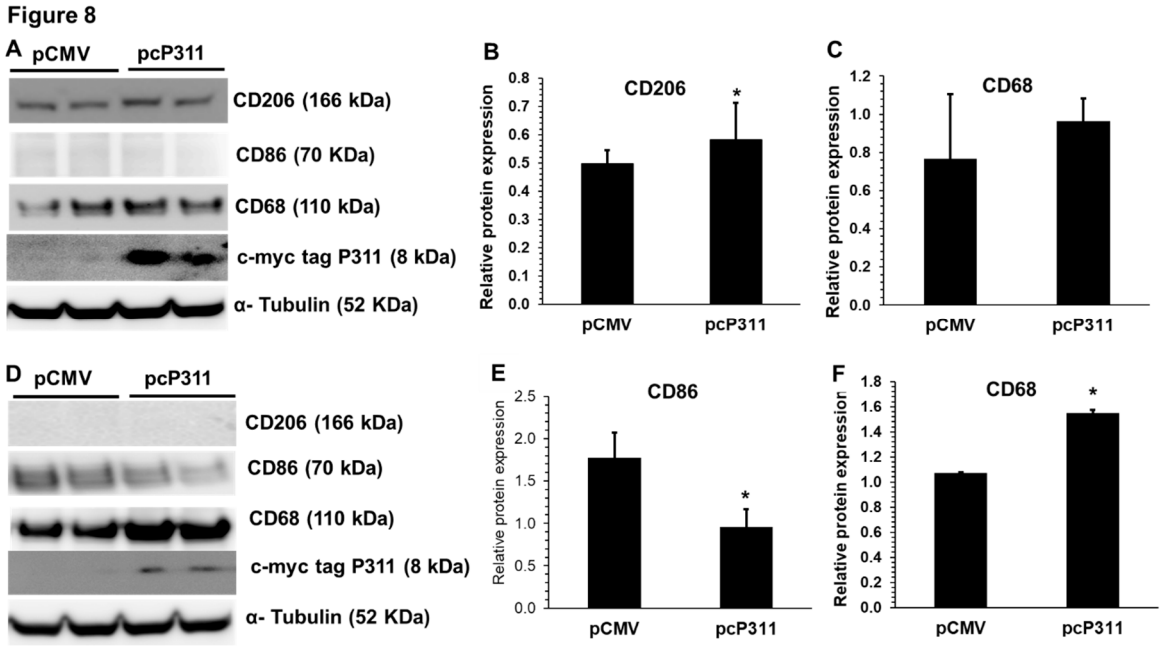

Figure 8. P311 expression induced anti-inflammatory roles by decreasing pro-inflammatory phenotype as well as increasing anti-inflammatory phenotype of RAW cells. A, D. Immunoblot analyses was performed to verify the expression of CD206 (M2 marker), CD86 (M1 marker), CD68 (pan macrophage marker) and c-myc tag P311 in IL4 treated (A) and LPS treated (D), pCMV and pcP311 transfected RAW cells. Lower panel represents loading control, α-tubulin. E-G. Densitometric quantitation of CD206 (B) and CD68 (C) or CD86 (E) and CD68 (F) proteins expression normalized to α-tubulin expression in IL4 and LPS treated pCMV and pcP311 transfected cells, respectively. Histograms represents mean ± S.D. *Represents statistical significance ($p<0.05$) between pcP311 vs. pCMV group.

There is a significant increase in the levels of CD206 in pcP311 transfected cells treated with IL4. However, IL4 treated cells did not show any expression of CD86 protein and there is no significant change in CD68 protein expression compared to controls. Whereas P311 overexpression in LPS treated cells showed no CD206 but showed significant decrease in CD86 protein expression compared with EV transfected control cells. However, there is an increase in the expression of CD68 in P311 overexpressed cells compared to EV control group treated with LPS. These results demonstrate that the P311 activates macrophages to M2-type macrophage phenotype and protects macrophages from inflammatory stimulants like LPS by curtailing pro-inflammatory M-1 type internal environment.

2.4. P311 Promotes Raw Cell Activation Towards M2 Phenotype Through Phosphorylation of STAT6

To understand the molecular mechanisms of role of P311 role on macrophage activation/ polarization, we studied related signaling molecules that include signal transducer and activator of transcription 6 (STAT6), signal transducer and activator of transcription 3 (STAT3) and I-kappa B alpha (IKB-α), the inhibitory subunit of NFκB signaling pathway. We studied the total and phosphorylation state of these signaling molecules in empty vector (pCMV) and P311 overexpressing pcP311 transfected RAW cells (Figure 9). The results demonstrated that there is a significant increase in the ratio of phosphorylated STAT6 to total STAT6 expression in pcP311 overexpression group when compared to pCMV control group. In contrast, there is no difference in the ratios of phosphorylated STAT3 to total STAT3 and phosphorylated IKB-α to total IKB-α between P311 overexpression group and control group. Collectively, these results indicate that P311 potentially induces M2-type macrophage polarization through the activation of STAT6 in canonical JAK-STAT6 signaling pathway.

 doi:10.20944/preprints202604.1556.v1

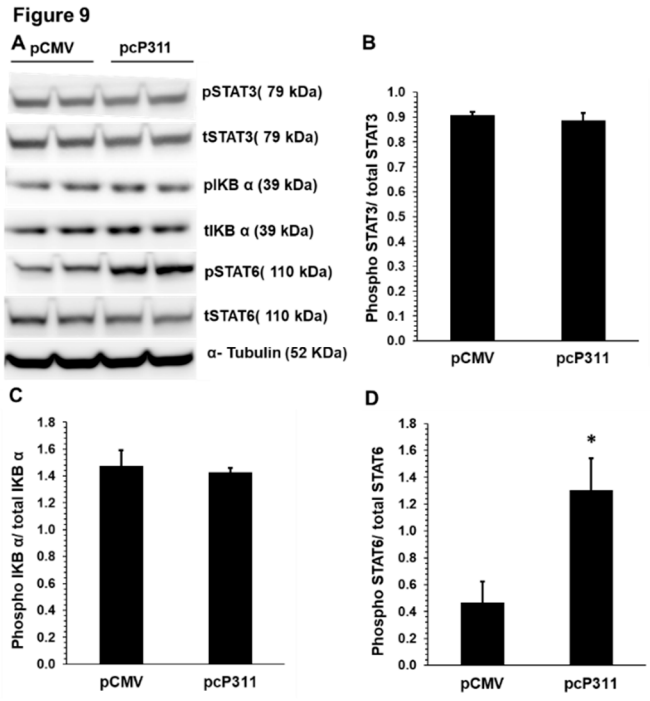

Figure 9. Molecular mechanisms of P311 mediated M2-type macrophage polarization. A. Immunoblot analyses was performed to verify the expression of phosphoSTAT3 (pSTAT3), totalSTAT3 (tSTAT3), phosphoIKBα (pIKBα), totalIKBα (tIKBα), phosphoSTAT6 (pSTAT6) and totalSTAT6 (tSTAT6) in pCMV and pcP311 transfected RAW cells. Lower panel represents loading control, α-tubulin. B-D. Densitometric quantitation of ratios of phospho- and total- proteins expression of STAT3 (B), IKBα (C) and STAT6 (D) normalized to α-tubulin expression in pCMV and pcP311 transfected cells, respectively. Histograms represents mean ± S.D. *Represents statistical significance ($p<0.05$) between pcP311 vs. pCMV group.

2.5. Loss of P311 Led to Gut Dysbiosis with Obese and Inflammatory Microbiome Compared to WT

Next, we used 16s rRNA to assess whether P311 affects the gut microbiome and if these changes reflect any changes in inflammation and overweight/obesity.

First, several beta metrics were examined to gauge dissimilarities in microbial communities between WT and P311 KOs. Looking at the Bray-Curtis measurement (Figure 10) which measures the numerical quantity of microbes and their abundances, using principal component plot (PCA) to display changes. There is a clear delineation between P311 KO's and WT microbial community composition (Figure 10A). We used the unweighted unifrac measurement where we saw a similar significant change in relatedness between the microbes between WT and P311 KO's (data not shown). The weighed unifrac measurements considers abundances increased similarities in composition. Next, we verified how phylogenetic relationships are altered in microbial communities with the loss of P311, we aggregated the amplicon sequence variants (ASVS) and grouped them based on their biological classification up to level 7 i.e., species level. This allow for the comparison of abundance distributions of the taxa between WT and P311KO as shown in Figure 10B.

 doi:10.20944/preprints202604.1556.v1

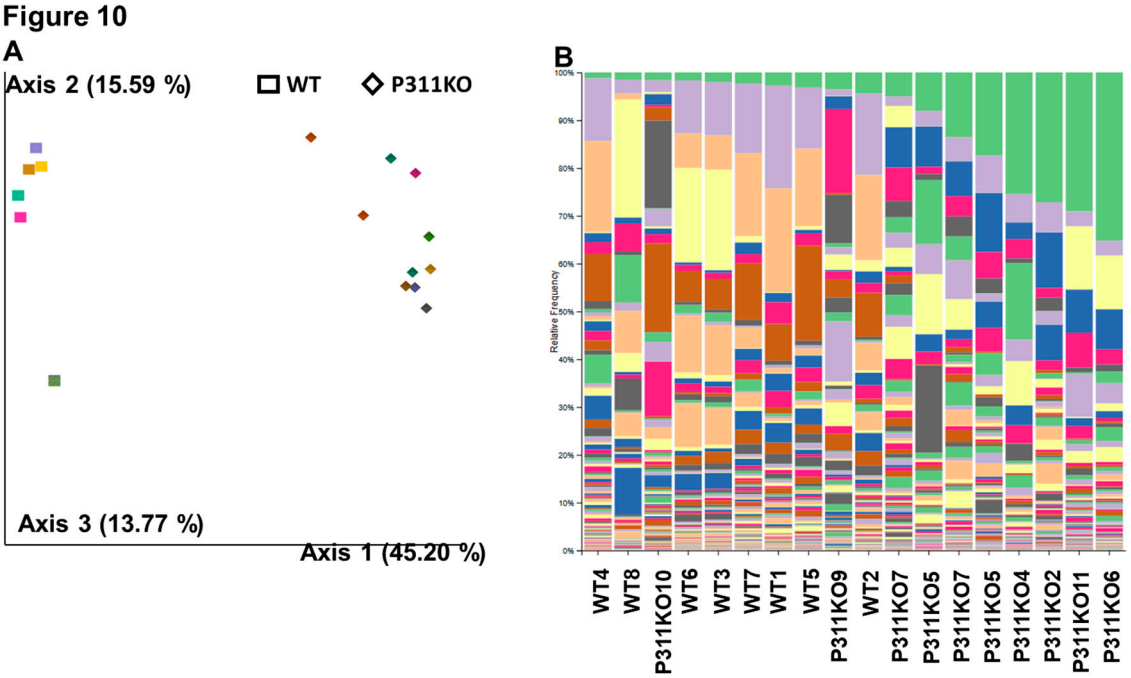

Figure 10. Microbial taxonomic diversity between WT and P311 KO mice. A. Bray–Curtis beta diversity among Wildtype (WT, n=8) and P311 knockout (KO, n=10) visualized via principal coordinate analysis (PCoA). Points represent individual fecal samples shaped by genotype (Wildtype: Square; P311 KO: Diamond). The three axes explain 45.20%, 15.59% and 13.77% of the total variance, respectively among samples. B. Taxonomic bar plot between Wildtype and P311 KO samples. The bar chart represents a depth of taxonomic identification up to Level 7 i.e species level. Bar length represents species relative abundance within each sample.

Further, we examined the diversity of the microbial flora between WT and P311 KOs. Looking at measures of alpha diversity, which measure species richness and evenness, P311 KO's have a decrease in species in diversity as related by the Chao index (Figure 11B) which heavily weights low abundance or rare species. Looking at measures of evenness which consider species abundance we observed decreases in Observed and Shannon measures (Figure 11A, C) in P311 KO compared to WT.

 doi:10.20944/preprints202604.1556.v1

Figure 11

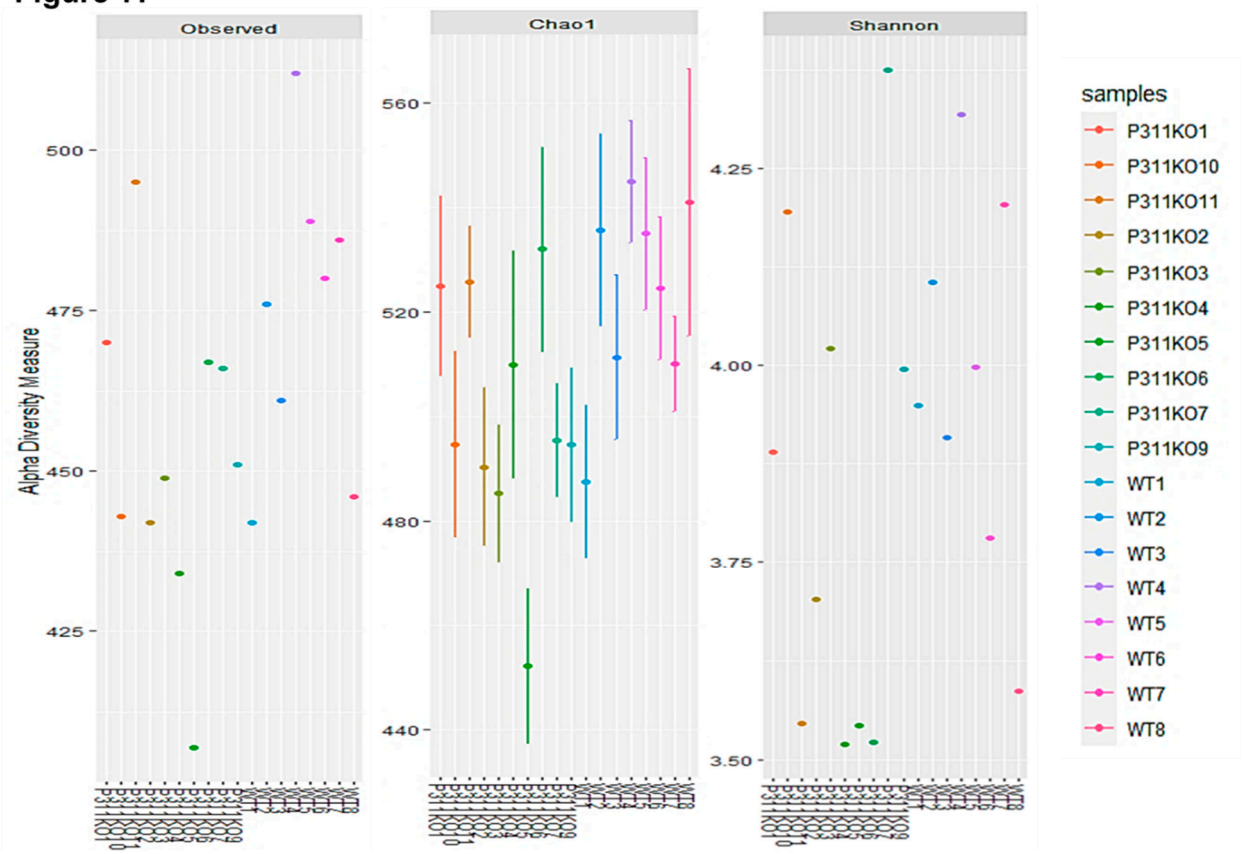

Figure 11. Alpha diversity metrics of gut microbiota between WT and P311 KO mice. A-C. Observed richness (A), Chao1 estimator of species richness (B), and Shannon diversity index (C) comparing alpha diversity of gut microbiota between Wildtype (WT) and P311 KO mice. Each point represents an individual sample, with colors corresponding to sample identifiers as indicated in the legend. In Fig 1B, points are shown with error bars representing variability associated with the Chao1 estimator. Observed richness counts total number of taxa and Chao1 indices indicate overall species richness, while the Shannon index accounts for both richness and evenness of microbial communities.

Figure 12A shows mean log fold change for major bacterial phyla comparing P311KOs and WTs. The positive values in the red indicate the enrichment in P311KO whereas the negative fold changes in teal color indicates the enrichment in WTs. Figure 12B shows the number of significantly altered Taxa within each phylum between P311KO (red) and WT (teal). Bars represents the counts of taxa which were statistically significant $p<0.5$. Firmicutes shows the greatest number of differentially abundant taxa with P311 deletion.

 doi:10.20944/preprints202604.1556.v1

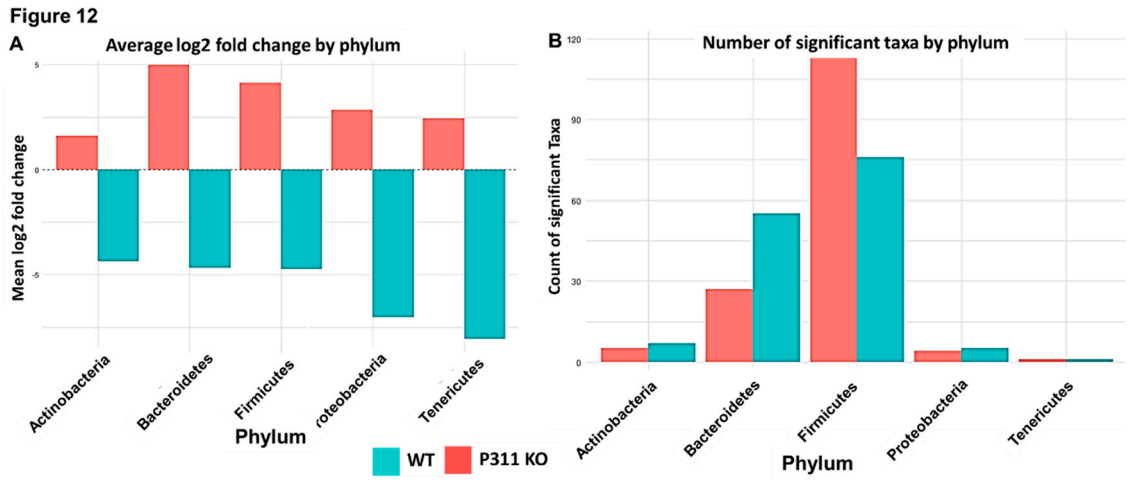

Figure 12. Differential microbial composition by phylum in WT and P311 KO groups. A. Mean log2 fold changes in relative abundance of major bacterial phyla comparing WT and P311 KO mice. Red bars indicate enrichment in P311 KO, whereas teal bars indicate enrichment in WT. B. Number of significantly altered microbial taxa within each phylum between WT and P311 KO groups. Bars represent counts of taxa meeting statistical significance criteria ($p < 0.05$).

Figure 13 shows the differences in abundance of Firmicutes and Bacteroidetes between P311KO compared to WT. Figure 13A-B shows the abundance of Firmicutes and Bacteroidetes from each individual animal of WTs and P311KOs. Genus Firmicutes showed increased presence in P311 KOs with a fold change of 4.5 ($p<0.05$) (Figure 13C). Genus Bacteroidetes had decreased presence with fold change -4.8 ($p<0.05$) (Figure 13D). The ratio of Firmicutes/Bacteroidetes is increased in P311 KOs compared to WT (1.11 vs 0.54 i.e., 0.48) (Figure 13E). Higher ratios have an association with inflammation and obesity can be an indicator of dysbiosis.

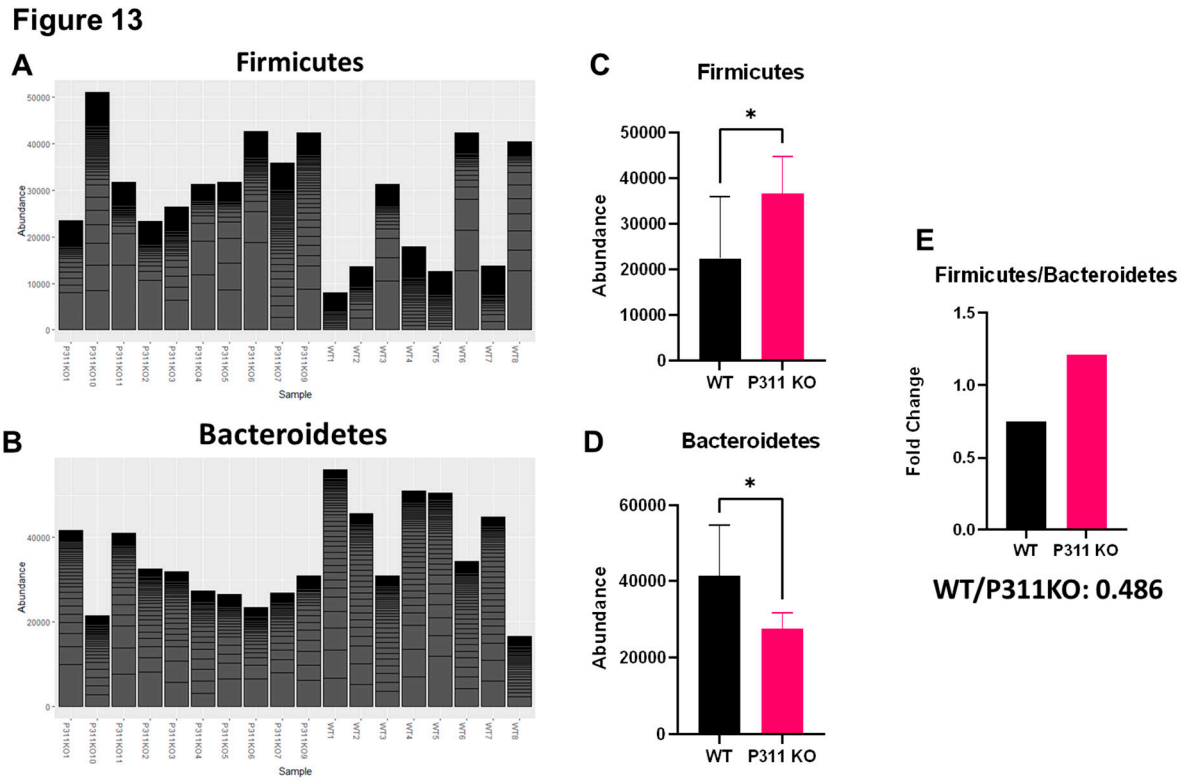

 doi:10.20944/preprints202604.1556.v1

Figure 13. Sample-level relative abundance of Firmicutes and Bacteroidetes in P311 knockout and wild-type mice. A-B. Stacked bar plots showing the relative abundance of *Firmicutes* (A, top) and *Bacteroidetes* (B, bottom) across individual samples from WT and P311 KO mice. Each bar represents a single sample and its corresponding abundance on the y-axis. C-D. total abundance numbers of Firmicutes and Bacteroidetes in WT and P311 KO samples ($p < 0.05$). E. Histogram showing the ratio of Firmicutes/Bacteroidetes between WT and P311 KO.

Looking at a plot of taxonomy distribution (Figure 14), we demonstrated that within Genus Firmicutes notable increase in *Lactobacillus murinus* and *Lactobacillus gasseri*. P311 KOs have a decrease in *Alloprevotella* which is a genus of anaerobic, gram-negative bacteria found in the human oral cavity and gut. It acts as a glycolytic bacterium, producing significant amounts of acetic and succinic acid, which help maintain intestinal barrier integrity and modulate metabolic processes. It functions to produce short-chain fatty acids (SCFAs)—specifically acetate and succinate—which contribute to gut health. We also observed decreases in *Bacteroides sartorii,* which plays a key role in breaking down complex plant polysaccharides and dietary fibers that human enzymes cannot digest and produce, acetate and propionate for energy use.

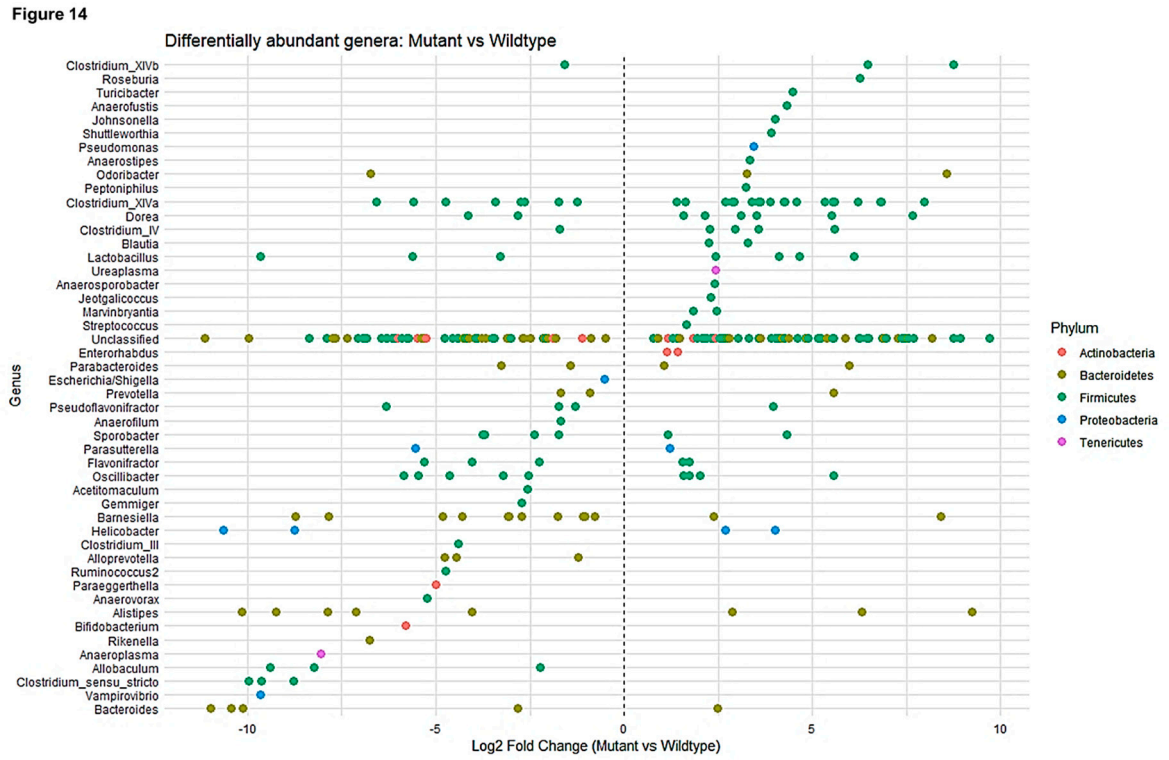

Figure 14. Genus-level differential abundance between WT and *P311* KO microbiomes. Genus-level differential abundance analysis showing log2 fold change between WT and P311 KO for individual taxa. Each point represents a genus, colored by phylum (Actinobacteria, Bacteroidetes, Firmicutes, Proteobacteria, and Tenericutes). The vertical dashed line at zero indicates no change between groups; points to the left indicate enrichment of respective microbes in WT and points to the right indicate enrichment of respective microbes in P311 KO.

3. Discussion

Previously our lab reported the key role of P311 in adipogenesis using 3T3L1 preadipocytes indicating the potential function of P311 in the regulation of white adipose tissue development [32,47,48]. A potential role of P311 in inflammation was predicted using *in silico* protein-protein interaction (PPI) network model [42]. As our ongoing studies and other studies showed the role of P311 in obesity and MASLD [32,47–49], current studies were conducted to shed light on the axis of

 doi:10.20944/preprints202604.1556.v1

P311, gut microbiome and inflammation (macrophage polarization). We examined RAW cells with different concentrations and exposure times of anti-inflammatory stimulant (IL4). Our results showed increased P311 expression matching with similar increases in CD206 (M2 marker) proportional to concentration of IL4 and similar results repeated with increased exposure time with IL4. To further understand the correlation between M2 phenotype and P311, we verified whether P311 overexpression have any effect on macrophage phenotypes in RAW cells. We noticed predominant expression of CD206 in P311 overexpressed RAW cells which is absent in control group. These results demonstrates that P311 protein independently influences the macrophage activation towards M2 phenotype. Our results concur with the wound healing and angiogenesis studies reported recently using a mice model [34]. Our additional studies verifying the effect of different concentration and exposure times of pro-inflammatory stimulant (LPS) on RAW cells showed switching of macrophages to M2-type inducing pro-inflammatory phenotype (increase CD86) with decrease in P311 transcripts. Here we have seen the inverse correlation between P311 expression and CD86 expression. Previous reports indicate that inflammatory effects of LPS vary with exposure time by counter mechanism of anti-inflammatory proteins such as IL10 and kinetics of signaling molecules [50]. Treating P311 overexpressing RAW cells with IL4 increased the anti-inflammatory roles of M2-macrophages significantly but less than the individual exposures (P311 or IL4). However, treating P311 overexpressing RAW cells with LPS significantly reduced pro-inflammatory phenotypic changes as indicated by the decrease in the expression of CD86 expression compared with control. Altogether these observations conclude that the P311 protein not only has an anti-inflammatory role on macrophages but also has inhibitory function on pro-inflammation.

We evaluated the CD68 marker as a pan macrophage marker which is also marker for CLS. We noticed that CD68 expression was significantly decreased at higher concentrations (above 50ng/mL, protein expression) and longer treatments (over 48 hours, both mRNA and protein levels) with LPS. These observations imply potential role of bacterial toxin LPS on not only increasing pro-inflammatory phenotype of macrophages, but LPS might be changing altogether the nature of macrophages to less macrophage-like cells or transdifferentiate into new cell types like myofibroblasts [51–53]. In addition, this might be associated with decreased phagocytic functions. CD68 is a well-known immune histological marker but mainly present in the endosomal/lysosomal compartment but shuttles to cell surface and acts as potent scavenger receptor [54] [54]. Its expression in lipid associated macrophages plays a key role in CLS for clearing cell debris, regulating phagocytosis, and recruiting macrophages [55].

Our understanding of the molecular mechanism on study findings showed P311 presence increased the expression of phosphor-STAT6, establishing the P311's association with JAK/STAT signaling pathway for alternative macrophage activation [56]. Other key signaling molecules, STAT3 and IKB-α (both total and phosphorylated forms) not show any differences. It indicates that the P311 association with STAT6 activation indirectly protects the macrophages leading them to anti-inflammatory phenotype.

The microbiome consisting of various bacteria, archaea, fungi, protozoa, and viruses has essential roles in the human organs and organ systems including digestion of biomolecules, production of vitamins and short chain fatty acids and energy homeostasis [24–26,28]. Loss of P311 shows a powerful ability to remodel the microbial gut community towards a microbial environment that supports energy storage rather than energy expenditure. This is most notably visible with the increased presence of the microbial genera Firmicutes in P311 KOs which is associated with the production of short chain fatty acids like butyrates, acetates, and propionates, through the fermentation of dietary fiber and resistant starches. The short chain fatty acids, primarily acetate, are converted into acetyl-CoA which is a precursor to long chain fatty acids and triglyceride production during lipogenesis [57]. Higher ratios of Firmicutes to Bacteroidetes is associated with obesity and a maker of gut dysbiosis [58]. In our data we see this ratio of (1.1 vs 0.54) in P311 KO's and WT respectively, indicating that *P311* plays a role in this switch in abundance.

 doi:10.20944/preprints202604.1556.v1

The connection between obesity and bacterial communities often entails a third axis associated with inflammatory pathways. Firmicutes from the class Negativicutes and Halanaerobiales increased lipopolysaccharide (LPS) production or its translocation, which activates macrophages via TLR4/NF-κB pathways to polarize macrophages toward the M1 phenotype, producing inflammatory cytokines TNF-α, IL-1β, and IL-6 [59,60]. This proinflammatory mechanism extends to disease states such as MASLD where increased presence of *Bacteroides vulgatus* was reported and saw inflammatory responses from Kupffer cells, neutrophils, and T cells [61]. In our data we observed low abundance of *Bacteroides vulgatus* (< 5) and increased abundance of genus *Bacteroides* in P311 KO mouse poops. Additional studies are underway to understand this connection. Increases in Firmicutes abundance have been associated with aging. The process of aging itself entails an inflammatory process promotes this along with decreased microbial diversity [57]. Looking at P311 KOs, we observed reduced diversity metrics which coupled with increased Firmicutes abundance creates potential dynamic of accelerated aging.

The gut microbiome has a complex interaction with inflammatory pathways by modulating immune functions through release of metabolites and structural components such as Pathogen-Associated Molecular Patterns (PAMPS) which both interact with and polarize macrophages [5]. Loss of P311 creates a system of dysbiosis in the GI by altering the gut microbiome composition, particularly with sharp increases in abundance of the genus Firmicutes. While microbial Firmicutes have been shown to promote anti-inflammatory processes through butyrate production promoting M2 polarization; excessive abundance of Firmicutes is associated with the obesogenic state which is a proinflammatory environment [62]. Firmicutes-derived metabolites like trimethylamine (TMA) a precursor to Trimethylamine N-oxide (TMAO) was reported to drive M1 polarization via NLRP3 inflammasome activation [63]. Furthermore, the imbalance in the P311KO microbial ecosystem creates an environment favoring short chain fatty acids producing microbes that perpetuate adipose tissue expansion. This dynamic creates a feedback loop supporting the release of adipokines e.g., leptin and resistin that promote M1 polarization in macrophages inducing the release of TNF-α and IL-6 triggering inflammatory pathways [64].

Overall, with the loss of P311 we observed a holistic shift in the microbial landscape that creates a dynamic conducive to inflammatory pathways driven by increases in lipogenic microbes. These microbes are already associated with the inflammation prone state of obesity and further exacerbate inflammatory pathways by driving M1 macrophage polarization as a byproduct of their increased abundance. The P311 KO microbe-obesity-inflammatory axis should be further explored to elucidate the mechanisms driving this phenomenon.

4. Materials & Methods

4.1. Cell Culture

a. Raw 264.7 mouse macrophages (Raw cells)

Raw 264.7 mouse macrophage cells (ATCC) were cultured in complete DMEM medium. To make complete DMEM medium, DMEM was supplemented with 10% fetal bovine serum (ATCC) and 1% Antibiotic-Antimycotic solution (Gibco, 100 U/mL of penicillin, 100 μg/mL of streptomycin and 0.25 μg/mL of amphotericin-B. The cells were maintained at 37 °C in a humidified atmosphere with 5% CO_2. All the experiments were conducted using cells in 4^{th} to 10^{th} passage.

b. Transfections

RAW 264.7 cells were seeded at a density of 2.0×10^6 to 3.0×10^6 in a 100mm culture dish. Cells were transfected with pCMV (empty vector) and c-myc-tag expressing pcP311 plasmid DNA [33] using lipofectamine 3000 reagent (Thermofisher Scientific, US) following the manufacturer optimized protocol. Transfected cells were used for experiments after 24 - 36 hours of transfection as detailed in individual experiments. Cells were harvested for qPCR and western blot analysis. Different transfection reagents Lipofectamine™ 2000 (Invitrogen), Lipofectamine™ 3000 (Invitrogen), Xfect™ Transfection Reagent (Takara Bio) and FuGENE® 6 Transfection Reagent (Promega Corporation)

 doi:10.20944/preprints202604.1556.v1

were used to optimize transfections in RAW cells. The Lipofectamine™ 3000 showed optimal efficiency and applied for further experiments.

4.2. Animal Studies

P311 KO mice are kind gift of Dr. Taylor as described earlier [33,65]. In brief, a major portion of *p311* gene, 4-kb SacI and NdeI fragment, covering most of the gene was replaced with pGKneoBpA plasmid. 3.9-kb and 4-kb size of noncoding regions both upstream and downs stream regions respectively of *p311* gene (SacI and NdeI fragment) were left intact.

4.3. Dose Dependent and Time Dependent Activation of Naïve Macrophages Using M1-Type Macrophage Phenotype Inducer (Lipopolysacharide) and M2-Type Macrophage Phenotype Inducer (Interleukin-4) on P311 Expression

a. Dose dependent effects of Lipopolysaccharide (LPS) concentrations on P311 expression.

Raw cells were treated with lipopolysaccharide (Sigma Aldric, MO, USA) at various concentrations 0, 10, 25, 50, 100 and 200 ng/mL for 24 hours. Cells were harvested at the end of incubation for quantitative PCR (qPCR) and western/immuno blot analysis.

b. Time dependent effects of Lipopolysaccharide (LPS) treatment on P311 expression.

Raw cells were incubated for 4, 9, 24, 48 and 72 hours with 100 ng/mL of LPS. At the end of each timepoint, cells were harvested for qPCR and western blot analysis.

c. Dose dependent effects of Interleukin 4 (IL-4) concentrations on P311 expression

Raw cells were treated with interleukin 4 (IL4, PeproTech, NJ, USA) at the concentrations of 0, 2, 5, 10, 20 and 50 ng/mL for 24 hours. Cells were harvested at the end of incubation for qPCR and western blot analysis.

d. Time dependent effects of Interleukin 4 (IL-4) treatment on P311 expression

Raw cells were incubated for 4, 9, 24, 48 and 72 hours with 10 ng/mL of IL-4. At the end of each time point, cells were harvested for qPCR and western blot analysis.

4.4. Quantitative Polymerase Chain Reaction (qPCR)

The qPCR analysis was performed as previously described [32,33,66]. In brief RNA isolations were performed using TRIzol reagent Invitrogen) followed by cDNA synthesis using iScript cDNA synthesis kit Bio-Rad Laboratories). Further qPCRs were performed using iQ SYBR Green Supermix Bio-Rad Laboratories) following manufacturer's instructions using a CFX Opus 96 Real-Time PCR System (Bio-Rad Laboratories). The following primers were used (Integrated DNA Technologies, Inc. USA). Anti-TATA binding protein (TBP) used as internal control to normalize the expression of mRNA transcripts and results were expressed as $2^{-\Delta\Delta CT}$.

P311 (NREP)	Forward: TGACCCAGACCAAGAGTTCT, Reverse: GCCGAGTGTAGAAAGCAGAG
CD206	Forward: CAAGTT GCCGTCTGA ACTGA, Reverse: TATCTCTGTCATCCCTGTCTCT
CD86	Forward: AAC AGCATCTGAGATCAGCA, Reverse: CAGACTCCTGTAGACGTGTTC
CD68	Forward: CCATGAATGTCCACTGTGCT, Reverse: CACCTGTCTCTCTCATTTCCTT

 doi:10.20944/preprints202604.1556.v1

TBP (normalization control)	Forward: CAGAACTGAAAATCAACGCAG, Reverse: TGTATCTACCGTGAATCTTGGC

4.5. Western Blot

Western blot analysis was conducted as described earlier [32,33,66]. Briefly, proteins were extracted using M-PER lysis buffer supplemented with Halt™ Protease Inhibitor Cocktail and 1% of TRITON X-100 (Thermo Scientific). Proteins were resolved on NuPAGE 4–12% Bis-Tris gels (Invitrogen) and transferred onto Immuno-Blot® PVDF membrane (Bio-Rad Laboratories). After blocking the membranes with 3% milk solution for at least 2 hours, the membranes were incubated with primary antibodies (1:1000 dilution unless otherwise mentioned) followed by horseradish peroxidase conjugated secondary antibodies (1:10,000 dilution). Supersignal west pico PLUS chemiluminescent substrate kit (Thermo Scientific) was used for image development and chemiluminescent protein bands visualization using LAS4000 gel imaging system (GE Healthcare) and/or iBright CL1500 Imaging System (Invitrogen). Primary antibodies details include anti-P311 (Abcam, Eugene, CA), anti-GAPDH (Abcam) and anti-c-myc Tag (Merck Millipore, Temecula, CA). And anti-CD206, anti-CD86, anti-CD68, anti-STAT6, anti-phospho-Stat6, anti-STAT3, anti-phospho-STAT3, anti-IKBα, anti-phospho-IKBα, anti-TBP and anti-α-Tubulin were purchased from cell signaling technology (Danvers, MA). Secondary antibodies, goat anti-rabbit IgG (H + L)-HRP conjugate and goat anti-mouse IgG (H + L)-HRP Conjugate were procured from Bio Rad Laboratories (Hercules, CA).

4.6. Flow Cytometry

Flowcytometric analysis was conducted for endogenous P311 expression and macrophage markers (CD206 and CD86) in pCMV and pcP311 transfected RAW cells. Briefly, cells were washed and prepared 1 X 10^6/mL cell suspension in FACS buffer (1%BSA in PBS). The cells were fixed with 4% paraformaldehyde, followed by permeabilized with 0.1% Triton-X in PBS. Cells were then incubated with primary antibodies (1:100 dilution) followed by incubated with fluorophore tagged secondary antibody (1:500 dilution). Immuno-stained cells resuspended in FACS buffer and analyzed using flow cytometry (Guava® easycyte, cytek). Primary antibodies anti-P311 (Abcam), anti-c-myc tag (Merck Millipore), and anti-CD206, anti-CD86, anti-F4/80 rabbit monoclonal antibody and anti-F4/80 rat monoclonal antibody (cell signaling technology) were used. Secondary antibodies goat anti-mouse IgG (H+L) Alexa Fluor™ 488 (Invitrogen), goat anti-rat IgG (H+L) Alexa Fluor™ 647 (Invitrogen), goat anti-rabbit IgG (H+L) Alexa Fluor™ 488 (Invitrogen), and goat anti-rabbit IgG (H+L) Alexa Fluor™ 647 (Invitrogen) were used species specific manner according to primary antibodies used.

4.7. Immunofluorescence (IF)

Endogenous P311 expression in RAW cells was studied using immunofluorescence method as described earlier [32,33,38]. RAW cells approximately 1.0 – 2.0X10^5 cells/mL seeded into chamber glass slides and treated with either LPS or IL4. Cells with vehicle treatment were used as controls. After 24 hours of treatment, cells were fixed with 4% paraformaldehyde, followed by permeabilized with 0.1% Triton-X in phosphate buffered saline (PBS) and blocked with 3% BSA in PBS. Cells were then incubated with P311 primary antibodies (Abcam) followed by incubation with Alexa Flur 488 goat anti rabbit IgG(H+L) secondary antibody (1:500 dilution, Invitrogen). Immuno-stained cells were mounted with ProLong Gold antifade mountant with 4′,6-diamidino-2-phenylindole (DAPI). Immunofluorescent images were captured with 40X objective in BZ-X810 fluorescence confocal microscope (Keyence corporation of America). Raw cells approximately 3.0X10^6 cells/mL were

 doi:10.20944/preprints202604.1556.v1

seeded into 100 mm cell culture dishes. After 24 hours of treatments of LPS and IL4 as well as a vehicle treatment (control), cells were harvested and used for immunoblot analysis.

4.8. Microbiome Studies & 16s rRNA Sequencing

Fecal samples were collected from wildtype and P311 KO mice (n= 8-10 animals) in accordance with Institutional Animal Care and Use Committee (IACUC) protocol and the samples were flash frozen in liquid nitrogen. Samples were sequenced at the UAB Microbiome Resource, Center for Clinical and Translational Sciences, University of Alabama at Birmingham following standard published protocol [67]. In brief, fecal samples were diluted in 20 ml of Cary-Blair medium to the final concentration of 0.1 mg/ml containing 10% of v/v glycerol. Five milliliter aliquots are dispensed into cryovial tubes and stored at −80°C until the use. DNA was isolated using the Fecal DNA Isolation Kit (Zymo Research). Primers specific for the V4 region of microbial DNA were used for amplification. PCR was performed using 3′ and 5′ primers both consisting of an adaptor sequence with and the 3′ end containing an additional 6-bp region for the "barcoded" index sequences using LongAmp Taq PCR kit (New England Bio). The PCR program include 1 cycle of 1 minute incubation at 94°C (initial denaturation); 32 cycles of 30 second incubation at 94°C, 1 minute incubation at 50°C and 1 minute incubation at 65°C; followed by 1 cycle incubation for 3 minutes at 65°C (final extension) and final hold at 4°C. The PCR products from the individual samples were electrophoresed on an agarose gel (1.0% agarose/Tris-borate-EDTA gel), visualized by UV illumination and gel extraction of amplicons was conducted using QIAquick Gel Extraction Kit (Qiagen). The purified amplicons were quantitated using Pico Green solution (Invitrogen) on an Infinite M200 fluorescent plate reader. Samples were then sequenced on Illumina MiSeq platform. QWRAP was used for data preprocessing as described in the protocol [67]. The package phyloseq was used for data analysis and ggplot2 for data visualization.

4.9. Data Analysis

Data was presented as Mean ± Standard deviation. Comparisons between groups were calculated using a two-tailed unpaired t-test. The p Value <0.05 considered as statistical significance. Each experiment was conducted in triplicates and repeated at least three times.

5. Conclusion

Our study findings suggest that P311 influence macrophage polarization towards anti-inflammatory M2-phenotype. Further, P311 can independently and in combination with bacterial toxin agent (LPS) is capable of suppressing the inflammatory phenotype. These findings direct our future research towards P311 associated macrophage roles during metabolic inflammation. P311KOs showed a change in GI microbiome towards obesogenic and inflammation prone states. The P311 KO microbe-obesity-inflammatory axis should be further explored to elucidate the mechanisms driving this phenomenon.

Authors Contribution: Conceptualization: K.B; writing – original draft preparation: S.B., S.M., P.K., and K.B.; writing – review and editing: K.B. Studies confuction and data collection: S.B., S.M., P.K. Data Analysis and Interpretation: S.B., S.M., P.K., and K.B. All authors have read and agreed to the published version of the manuscript.

Acknowledgments: This study was supported by SCORE/SC1 grant funding to KB (5SC1GM141937). Research reported in this publication was supported by the National Institute of General Medical Sciences of the National Institutes of Health under Award Number SC1GM141937. The content is solely the responsibility of the authors and does not necessarily represent the official views of the National Institutes of Health. SM is RISE Fellow supported by NIGMS, R25GM058268. We acknowledge the support of MSM Core Facility (supported by NIMHD, 5U54MD0076037). We acknowledge the services and support of Dr. Casey D. Morrow, Dr. Peter G

 doi:10.20944/preprints202604.1556.v1

Eipers and UAB Microbiome Resource at University of Alabama at Birmingham, Birmingham, AL towards microbiome studies.

Conflicht of Interest: The authors declare no conflict of interest.

References

1. Bluher, M. Obesity: global epidemiology and pathogenesis. *Nat Rev Endocrinol* **2019**, *15* (5), 288-298. DOI: 10.1038/s41574-019-0176-8 From NLM Medline.
2. WHO. Obesity: preventing and managing the global epidemic. Report of a WHO consultation. *World Health Organ Tech Rep Ser* **2000**, *894*, i-xii, 1-253.
3. Daley, V. S. C. S. F. *Secondary causes of obesity and comprehensive diagnostic evaluation*; StatPearls Publishing, 2025.
4. Fontaine, K. R.; Redden, D. T.; Wang, C.; Westfall, A. O.; Allison, D. B. Years of life lost due to obesity. *JAMA* **2003**, *289* (2), 187-193. DOI: 10.1001/jama.289.2.187.
5. Aleksandrova, K.; Egea Rodrigues, C.; Floegel, A.; Ahrens, W. Omics Biomarkers in Obesity: Novel Etiological Insights and Targets for Precision Prevention. *Curr Obes Rep* **2020**, *9* (3), 219-230. DOI: 10.1007/s13679-020-00393-y.
6. Kaplan, M. S.; Huguet, N.; Newsom, J. T.; McFarland, B. H.; Lindsay, J. Prevalence and correlates of overweight and obesity among older adults: findings from the Canadian National Population Health Survey. *J Gerontol A Biol Sci Med Sci* **2003**, *58* (11), 1018-1030. DOI: 10.1093/gerona/58.11.m1018.
7. Stierman, B.; Afful, J.; Carroll, M. D.; Chen, T. C.; Davy, O.; Fink, S.; Fryar, C. D.; Gu, Q.; Hales, C. M.; Hughes, J. P.; et al. National Health and Nutrition Examination Survey 2017-March 2020 Prepandemic Data Files-Development of Files and Prevalence Estimates for Selected Health Outcomes. *Natl Health Stat Report* **2021**, (158). DOI: 10.15620/cdc:106273.
8. Chatzigeorgiou, A.; Karalis, K. P.; Bornstein, S. R.; Chavakis, T. Lymphocytes in obesity-related adipose tissue inflammation. *Diabetologia* **2012**, *55* (10), 2583-2592. DOI: 10.1007/s00125-012-2607-0.
9. Kanneganti, T. D.; Dixit, V. D. Immunological complications of obesity. *Nat Immunol* **2012**, *13* (8), 707-712. DOI: 10.1038/ni.2343.
10. McLaughlin, T.; Ackerman, S. E.; Shen, L.; Engleman, E. Role of innate and adaptive immunity in obesity-associated metabolic disease. *J Clin Invest* **2017**, *127* (1), 5-13. DOI: 10.1172/JCI88876.
11. Kloting, N.; Bluher, M. Adipocyte dysfunction, inflammation and metabolic syndrome. *Rev Endocr Metab Disord* **2014**, *15* (4), 277-287. DOI: 10.1007/s11154-014-9301-0.
12. Sun, K.; Kusminski, C. M.; Scherer, P. E. Adipose tissue remodeling and obesity. *J Clin Invest* **2011**, *121* (6), 2094-2101. DOI: 10.1172/JCI45887.
13. Weisberg, S. P.; McCann, D.; Desai, M.; Rosenbaum, M.; Leibel, R. L.; Ferrante, A. W., Jr. Obesity is associated with macrophage accumulation in adipose tissue. *J Clin Invest* **2003**, *112* (12), 1796-1808. DOI: 10.1172/JCI19246.
14. Russell, D. G.; Huang, L.; VanderVen, B. C. Immunometabolism at the interface between macrophages and pathogens. *Nat Rev Immunol* **2019**, *19* (5), 291-304. DOI: 10.1038/s41577-019-0124-9.
15. Cassetta, L.; Cassol, E.; Poli, G. Macrophage polarization in health and disease. *ScientificWorldJournal* **2011**, *11*, 2391-2402. DOI: 10.1100/2011/213962.
16. Murray, P. J.; Allen, J. E.; Biswas, S. K.; Fisher, E. A.; Gilroy, D. W.; Goerdt, S.; Gordon, S.; Hamilton, J. A.; Ivashkiv, L. B.; Lawrence, T.; et al. Macrophage activation and polarization: nomenclature and experimental guidelines. *Immunity* **2014**, *41* (1), 14-20. DOI: 10.1016/j.immuni.2014.06.008.
17. Shapouri-Moghaddam, A.; Mohammadian, S.; Vazini, H.; Taghadosi, M.; Esmaeili, S. A.; Mardani, F.; Seifi, B.; Mohammadi, A.; Afshari, J. T.; Sahebkar, A. Macrophage plasticity, polarization, and function in health and disease. *J Cell Physiol* **2018**, *233* (9), 6425-6440. DOI: 10.1002/jcp.26429.
18. Biswas, S. K.; Mantovani, A. Orchestration of metabolism by macrophages. *Cell Metab* **2012**, *15* (4), 432-437. DOI: 10.1016/j.cmet.2011.11.013.

 doi:10.20944/preprints202604.1556.v1

19. Jetten, N.; Verbruggen, S.; Gijbels, M. J.; Post, M. J.; De Winther, M. P.; Donners, M. M. Anti-inflammatory M2, but not pro-inflammatory M1 macrophages promote angiogenesis in vivo. *Angiogenesis* **2014**, *17* (1), 109-118. DOI: 10.1007/s10456-013-9381-6.
20. Wang, N.; Liang, H.; Zen, K. Molecular mechanisms that influence the macrophage m1-m2 polarization balance. *Front Immunol* **2014**, *5*, 614. DOI: 10.3389/fimmu.2014.00614.
21. Zeyda, M.; Gollinger, K.; Kriehuber, E.; Kiefer, F. W.; Neuhofer, A.; Stulnig, T. M. Newly identified adipose tissue macrophage populations in obesity with distinct chemokine and chemokine receptor expression. *Int J Obes (Lond)* **2010**, *34* (12), 1684-1694. DOI: 10.1038/ijo.2010.103.
22. Chylikova, J.; Dvorackova, J.; Tauber, Z.; Kamarad, V. M1/M2 macrophage polarization in human obese adipose tissue. *Biomed Pap Med Fac Univ Palacky Olomouc Czech Repub* **2018**, *162* (2), 79-82. DOI: 10.5507/bp.2018.015.
23. Sica, A.; Mantovani, A. Macrophage plasticity and polarization: in vivo veritas. *J Clin Invest* **2012**, *122* (3), 787-795. DOI: 10.1172/JCI59643.
24. Clarridge, J. E., 3rd. Impact of 16S rRNA gene sequence analysis for identification of bacteria on clinical microbiology and infectious diseases. *Clin Microbiol Rev* **2004**, *17* (4), 840-862, table of contents. DOI: 10.1128/CMR.17.4.840-862.2004.
25. Jensen, B. A. H.; Heyndrickx, M.; Jonkers, D.; Mackie, A.; Millet, S.; Naghibi, M.; Paerregaard, S. I.; Pot, B.; Saulnier, D.; Sina, C.; et al. Small intestine vs. colon ecology and physiology: Why it matters in probiotic administration. *Cell Rep Med* **2023**, *4* (9), 101190. DOI: 10.1016/j.xcrm.2023.101190.
26. Rowland, I.; Gibson, G.; Heinken, A.; Scott, K.; Swann, J.; Thiele, I.; Tuohy, K. Gut microbiota functions: metabolism of nutrients and other food components. *Eur J Nutr* **2018**, *57* (1), 1-24. DOI: 10.1007/s00394-017-1445-8.
27. Lawal, S. A.; Voisin, A.; Olof, H.; Bording-Jorgensen, M.; Armstrong, H. Diversity of the microbiota communities found in the various regions of the intestinal tract in healthy individuals and inflammatory bowel diseases. *Front Immunol* **2023**, *14*, 1242242. DOI: 10.3389/fimmu.2023.1242242.
28. Lozupone, C. A.; Stombaugh, J. I.; Gordon, J. I.; Jansson, J. K.; Knight, R. Diversity, stability and resilience of the human gut microbiota. *Nature* **2012**, *489* (7415), 220-230. DOI: 10.1038/nature11550.
29. Matchado, M. S.; Ruhlemann, M.; Reitmeier, S.; Kacprowski, T.; Frost, F.; Haller, D.; Baumbach, J.; List, M. On the limits of 16S rRNA gene-based metagenome prediction and functional profiling. *Microb Genom* **2024**, *10* (2). DOI: 10.1099/mgen.0.001203.
30. Perez-Cobas, A. E.; Gomez-Valero, L.; Buchrieser, C. Metagenomic approaches in microbial ecology: an update on whole-genome and marker gene sequencing analyses. *Microb Genom* **2020**, *6* (8). DOI: 10.1099/mgen.0.000409.
31. Wastyk, H. C.; Fragiadakis, G. K.; Perelman, D.; Dahan, D.; Merrill, B. D.; Yu, F. B.; Topf, M.; Gonzalez, C. G.; Van Treuren, W.; Han, S.; et al. Gut-microbiota-targeted diets modulate human immune status. *Cell* **2021**, *184* (16), 4137-4153 e4114. DOI: 10.1016/j.cell.2021.06.019.
32. Nunez, S.; Young, C.; Adebayo, O.; Muppuru, K. M.; Badri, K. R. P311, a novel intrinsically disordered protein, regulates adipocyte development. *Biochem Biophys Res Commun* **2019**, *515* (1), 234-240. DOI: 10.1016/j.bbrc.2019.05.105.
33. Badri, K. R.; Yue, M.; Carretero, O. A.; Aramgam, S. L.; Cao, J.; Sharkady, S.; Kim, G. H.; Taylor, G. A.; Byron, K. L.; Schuger, L. Blood pressure homeostasis is maintained by a P311-TGF-beta axis. *J Clin Invest* **2013**, *123* (10), 4502-4512. DOI: 10.1172/JCI69884.
34. Chen, C.; Tang, Y.; Zhu, X.; Yang, J.; Liu, Z.; Chen, Y.; Wang, J.; Shang, R.; Zheng, W.; Zhang, X.; et al. P311 Promotes IL-4 Receptor–Mediated M2 Polarization of Macrophages to Enhance Angiogenesis for Efficient Skin Wound Healing. *J Invest Dermatol* **2023**, *143* (4), 648-660 e646. DOI: 10.1016/j.jid.2022.09.659.
35. Lagares, D. P311 in Scar Wars: Myofibroblasts Lost without Transforming Growth Factor beta Translation. *Am J Respir Cell Mol Biol* **2019**, *60* (2), 139-140. DOI: 10.1165/rcmb.2018-0255ED From NLM Medline.
36. Leung, J. K.; Cases, S.; Vu, T. H. P311 functions in an alternative pathway of lipid accumulation that is induced by retinoic acid. *J Cell Sci* **2008**, *121* (Pt 16), 2751-2758. DOI: 10.1242/jcs.027151.

 doi:10.20944/preprints202604.1556.v1

37. Pan, D.; Zhe, X.; Jakkaraju, S.; Taylor, G. A.; Schuger, L. P311 induces a TGF-beta1-independent, nonfibrogenic myofibroblast phenotype. *J Clin Invest* **2002**, *110* (9), 1349-1358. DOI: 10.1172/JCI15614 From NLM Medline.
38. Shi, J.; Badri, K. R.; Choudhury, R.; Schuger, L. P311-induced myofibroblasts exhibit ameboid-like migration through RalA activation. *Exp Cell Res* **2006**, *312* (17), 3432-3442. DOI: 10.1016/j.yexcr.2006.07.016.
39. Aramgam, S. L., Vaddi. D.R., Badri, K.R. P311 KO Mice are Protected from Experimentally Induced Lung Fibrosis. *Physiology* **2024**, *39*, 2585. DOI: https://doi.org/10.1152/physiol.2024.39.S1.25.
40. Badri, M. R., Kach, J., Aramgam, S.L., Sandbo, N.K., Schuger, L. P311, A New Key Player In The Pathogenesis Of Pulmonary Fibrosis. *Am J Respir Crit Care Med* **2013**, *187*, A5602. DOI: https://doi.org/10.1164/ajrccm-conference.2013.187.1_MeetingAbstracts.A5602.
41. Fujitani, M.; Yamagishi, S.; Che, Y. H.; Hata, K.; Kubo, T.; Ino, H.; Tohyama, M.; Yamashita, T. P311 accelerates nerve regeneration of the axotomized facial nerve. *J Neurochem* **2004**, *91* (3), 737-744. DOI: 10.1111/j.1471-4159.2004.02738.x From NLM Medline.
42. Wang, S.; Zhang, X.; Hao, F.; Li, Y.; Sun, C.; Zhan, R.; Wang, Y.; He, W.; Li, H.; Luo, G. Reconstruction and Functional Annotation of P311 Protein-Protein Interaction Network Reveals Its New Functions. *Front Genet* **2019**, *10*, 109. DOI: 10.3389/fgene.2019.00109 From NLM PubMed-not-MEDLINE.
43. Fujihara, M.; Muroi, M.; Tanamoto, K.; Suzuki, T.; Azuma, H.; Ikeda, H. Molecular mechanisms of macrophage activation and deactivation by lipopolysaccharide: roles of the receptor complex. *Pharmacol Ther* **2003**, *100* (2), 171-194. DOI: 10.1016/j.pharmthera.2003.08.003.
44. Raetz, C. R. Biochemistry of endotoxins. *Annu Rev Biochem* **1990**, *59*, 129-170. DOI: 10.1146/annurev.bi.59.070190.001021.
45. Gadani, S. P.; Cronk, J. C.; Norris, G. T.; Kipnis, J. IL-4 in the brain: a cytokine to remember. *J Immunol* **2012**, *189* (9), 4213-4219. DOI: 10.4049/jimmunol.1202246.
46. Liu, L.; Guo, H.; Song, A.; Huang, J.; Zhang, Y.; Jin, S.; Li, S.; Zhang, L.; Yang, C.; Yang, P. Progranulin inhibits LPS-induced macrophage M1 polarization via NF-small ka, CyrillicB and MAPK pathways. *BMC Immunol* **2020**, *21* (1), 32. DOI: 10.1186/s12865-020-00355-y.
47. Badri, K. R., White, D. Molecular Mechanisms of P311 on White Adipogenesis. *FASEB J* **2020**, *34*. DOI: https://doi.org/10.1096/fasebj.2020.34.s1.09018Digital Object Identifier (DOI).
48. Badri, K. R. Role of P311 in Adipocyte Plasticity and Metabolic Regulation. *Diabetes* **2022**, *71*, 234-LB. DOI: https://doi.org/10.2337/db22-234-LB.
49. De Jesus, D. F.; Kimura, T.; Gupta, M. K.; Kulkarni, R. N. NREP contributes to development of NAFLD by regulating one-carbon metabolism in primary human hepatocytes. *Cell Chem Biol* **2023**, *30* (9), 1144-1155 e1144. DOI: 10.1016/j.chembiol.2023.06.001 From NLM Medline.
50. Hobbs, S.; Reynoso, M.; Geddis, A. V.; Mitrophanov, A. Y.; Matheny, R. W., Jr. LPS-stimulated NF-kappaB p65 dynamic response marks the initiation of TNF expression and transition to IL-10 expression in RAW 264.7 macrophages. *Physiol Rep* **2018**, *6* (21), e13914. DOI: 10.14814/phy2.13914.
51. Shen, S.; Wang, L.; Liu, Q.; Wang, X.; Yuan, Q.; Zhao, Y.; Hu, H.; Ma, L. Macrophage-to-myofibroblast transition and its role in cardiac fibrosis. *Int Immunopharmacol* **2025**, *146*, 113873. DOI: 10.1016/j.intimp.2024.113873 From NLM Medline.
52. Wang, Y. Y.; Jiang, H.; Pan, J.; Huang, X. R.; Wang, Y. C.; Huang, H. F.; To, K. F.; Nikolic-Paterson, D. J.; Lan, H. Y.; Chen, J. H. Macrophage-to-Myofibroblast Transition Contributes to Interstitial Fibrosis in Chronic Renal Allograft Injury. *J Am Soc Nephrol* **2017**, *28* (7), 2053-2067. DOI: 10.1681/ASN.2016050573 From NLM Medline.
53. Zhuang, T.; Chen, M. H.; Wu, R. X.; Wang, J.; Hu, X. D.; Meng, T.; Wu, A. H.; Li, Y.; Yang, Y. F.; Lei, Y.; et al. ALKBH5-mediated m6A modification of IL-11 drives macrophage-to-myofibroblast transition and pathological cardiac fibrosis in mice. *Nat Commun* **2024**, *15* (1), 1995. DOI: 10.1038/s41467-024-46357-x From NLM Medline.
54. Chistiakov, D. A.; Killingsworth, M. C.; Myasoedova, V. A.; Orekhov, A. N.; Bobryshev, Y. V. CD68/macrosialin: not just a histochemical marker. *Lab Invest* **2017**, *97* (1), 4-13. DOI: 10.1038/labinvest.2016.116.

 doi:10.20944/preprints202604.1556.v1

55. Jia, Q.; Morgan-Bathke, M. E.; Jensen, M. D. Adipose tissue macrophage burden, systemic inflammation, and insulin resistance. *Am J Physiol Endocrinol Metab* **2020**, *319* (2), E254-E264. DOI: 10.1152/ajpendo.00109.2020.
56. Villarino, A. V.; Kanno, Y.; Ferdinand, J. R.; O'Shea, J. J. Mechanisms of Jak/STAT signaling in immunity and disease. *J Immunol* **2015**, *194* (1), 21-27. DOI: 10.4049/jimmunol.1401867.
57. Fusco, W.; Lorenzo, M. B.; Cintoni, M.; Porcari, S.; Rinninella, E.; Kaitsas, F.; Lener, E.; Mele, M. C.; Gasbarrini, A.; Collado, M. C.; et al. Short-Chain Fatty-Acid-Producing Bacteria: Key Components of the Human Gut Microbiota. *Nutrients* **2023**, *15* (9). DOI: 10.3390/nu15092211.
58. Magne, F.; Gotteland, M.; Gauthier, L.; Zazueta, A.; Pesoa, S.; Navarrete, P.; Balamurugan, R. The Firmicutes/Bacteroidetes Ratio: A Relevant Marker of Gut Dysbiosis in Obese Patients? *Nutrients* **2020**, *12* (5). DOI: 10.3390/nu12051474.
59. Antunes, L. C.; Poppleton, D.; Klingl, A.; Criscuolo, A.; Dupuy, B.; Brochier-Armanet, C.; Beloin, C.; Gribaldo, S. Phylogenomic analysis supports the ancestral presence of LPS-outer membranes in the Firmicutes. *Elife* **2016**, *5*. DOI: 10.7554/eLife.14589.
60. Meng, F.; Lowell, C. A. Lipopolysaccharide (LPS)-induced macrophage activation and signal transduction in the absence of Src-family kinases Hck, Fgr, and Lyn. *J Exp Med* **1997**, *185* (9), 1661-1670. DOI: 10.1084/jem.185.9.1661.
61. Nagashimada, M.; Honda, M. Effect of Microbiome on Non-Alcoholic Fatty Liver Disease and the Role of Probiotics, Prebiotics, and Biogenics. *Int J Mol Sci* **2021**, *22* (15). DOI: 10.3390/ijms22158008.
62. Duan, H.; Wang, L.; Huangfu, M.; Li, H. The impact of microbiota-derived short-chain fatty acids on macrophage activities in disease: Mechanisms and therapeutic potentials. *Biomed Pharmacother* **2023**, *165*, 115276. DOI: 10.1016/j.biopha.2023.115276 From NLM Medline.
63. Abudureheman, D.; Janaerbieke, S.; Song, Y.; Han, S.; Yimaer, W.; Wang, H. Mechanisms and Intervention Strategies of Trimethylamine N-Oxide in Abdominal Aortic Aneurysm. *Cardiology* **2025**, 1-20. DOI: 10.1159/000546190 From NLM Publisher.
64. Taylor, E. B. The complex role of adipokines in obesity, inflammation, and autoimmunity. *Clin Sci (Lond)* **2021**, *135* (6), 731-752. DOI: 10.1042/CS20200895 From NLM Medline.
65. Taylor, G. A.; Rodriguiz, R. M.; Greene, R. I.; Daniell, X.; Henry, S. C.; Crooks, K. R.; Kotloski, R.; Tessarollo, L.; Phillips, L. E.; Wetsel, W. C. Behavioral characterization of P311 knockout mice. *Genes Brain Behav* **2008**, *7* (7), 786-795. DOI: 10.1111/j.1601-183X.2008.00420.x From NLM Medline.
66. Badri, K. R.; Zhou, Y.; Dhru, U.; Aramgam, S.; Schuger, L. Effects of the SANT domain of tension-induced/inhibited proteins (TIPs), novel partners of the histone acetyltransferase p300, on p300 activity and TIP-6-induced adipogenesis. *Mol Cell Biol* **2008**, *28* (20), 6358-6372. DOI: 10.1128/MCB.00333-08.
67. Kumar, R.; Eipers, P.; Little, R. B.; Crowley, M.; Crossman, D. K.; Lefkowitz, E. J.; Morrow, C. D. Getting started with microbiome analysis: sample acquisition to bioinformatics. *Curr Protoc Hum Genet* **2014**, *82*, 18 18 11-18 18 29. DOI: 10.1002/0471142905.hg1808s82.